The efficient delivery of highly-siderophile elements to the core creates a mass accretion catastrophe for the Earth

Richard J. Anslow[1], Maylis Landeau[2], Amy Bonsor[1], Jonathan Itcovitz[1,3], Oliver Shorttle[1,4]

[1]Institute of Astronomy, University of Cambridge, Madingley Road, Cambridge, CB3 0HA, UK
[2]Université de Paris, Institut de Physique du Globe de Paris, CNRS, Paris, France
[3]Department of Civil and Environmental Engineering, Imperial College London, London, SW7 2AZ, UK
[4]Department of Earth Sciences, University of Cambridge, Downing Street, Cambridge, CB3 9ET, UK

Key Points:

- The entrainment of metal, and its HSE content, in a magma pond is possible only for $\leq$ 0.01 mm droplets.
- Metal delivered by $\geq$ 1 km impactors is lost to Earth's core, yet constraints on total mass accretion prevents HSE delivery by $\leq$ 1 km impactors.
- Thus, either an oxidized late veneer or the disruption of large impactors into $\leq$ 0.01 mm droplets is required to account for observed HSEs.

Corresponding author: Richard J. Anslow, `rja92@ast.cam.ac.uk`

Abstract

The excess abundance of highly siderophile elements (HSEs), as inferred for the terrestrial planets and the Moon, is thought to record a 'late veneer' of impacts after the giant impact phase of planet formation. Estimates for total mass accretion during this period typically assume all HSEs delivered remain entrained in the mantle. Here, we present an analytical discussion of the fate of liquid metal diapirs in both a magma pond and a solid mantle, and show that metals from impactors larger than approximately 1 km will sink to Earth's core, leaving no HSE signature in the mantle. However, by considering a collisional size distribution, we show that to deliver sufficient mass in small impactors to account for Earth's HSEs, there will be an implausibly large mass delivered by larger bodies, the metallic fraction of which lost to Earth's core. There is therefore a contradiction between observed concentrations of HSEs, the geodynamics of metal entrainment, and estimates of total mass accretion during the late veneer. To resolve this paradox, and avoid such a mass accretion catastrophe, our results suggest that large impactors must contribute to observed HSE signatures. For these HSEs to be entrained in the mantle, either some mechanism(s) must efficiently disrupt impactor core material into ≤ 0.01 mm fragments, or alternatively Earth accreted a significant mass fraction of oxidised (carbonaceous chondrite-like) material during the late veneer. Estimates of total mass accretion accordingly remain unconstrained, given uncertainty in both the efficiency of impactor core fragmentation, and the chemical composition of the late veneer.

Plain Language Summary

Highly siderophile elements (HSEs) have a very strong tendency to partition into planetary cores, rather than mantles. If Earth's mantle and core were chemically equilibrated, these elements should be almost non-existent in the mantle. Yet, these elements are much more abundant in the mantle than expected, and are present in roughly the same relative abundance as in chondritic meteorites. A widely-admitted hypothesis is that these elements were delivered as a 'late veneer' of chondritic material, carrying about 0.5 % of Earth's mass after core formation was complete. This estimate assumes that all HSEs delivered during the late veneer remained suspended in Earth's mantle. In this work, we show that it is very challenging for these elements, delivered by planetesimals larger than approximately 1 km, to avoid sinking to Earth's core, due to the large density of these metals relative to Earth's silicate mantle. Our calculations further show, by considering a realistic planetesimal size distribution, that there is insufficient mass in small planetesimals to account for Earth's HSEs. These results therefore highlight a contradiction between estimates of mass accretion during the late veneer, and our understanding of metal delivery to Earth's mantle.

1 Introduction

Highly siderophile elements (HSEs; namely Pt-group elements, Re and Au) have a very strong affinity for Fe-metal at low pressure, and should therefore be stripped from the molten silicate mantle during core formation. Partitioning data predict that HSEs should be both virtually non-existent in Earth's mantle, and, in those that remain, chemically fractionated according to their different affinities for metal (Righter et al., 2008; Mann et al., 2012). In contrast to these two predictions, the Earth's mantle contains a significant excess of HSEs compared to that expected from metal-silicate equilibration (Day et al., 2007; Walker, 2009), and these HSEs are found to be in nearly chondritic relative abundance (Day et al., 2016). The simplest explanation for these observations is the delivery of a 'late veneer' of chondritic material, with total mass $\sim 0.3-0.7$ % of the Earth (Kimura et al., 1974; Chou, 1978; Walker, 2009), overprinting the mantle's post-core formation HSE composition.

Further evidence in support of a significant, and widespread period of late accretion is that excess HSEs are also found, in broadly chondritic relative abundance, in the mantles of much smaller planetary bodies including the Moon (Day et al., 2007), Mars (Brandon et al., 2000, 2012), and Vesta (Dale et al., 2012). This strongly indicates that high-pressure equilibration does not alone control observed concentrations of HSEs in these bodies, since it appears unlikely that pressure-temperature conditions were the same at the bottom of these respective magma oceans. Thus, despite measurements indicating that the affinity of HSEs for metal decreases in high pressure-temperature conditions (Righter et al., 2008; Mann et al., 2012; Suer et al., 2021), a chondritic late veneer still appears necessary in order to account for the abundance of HSEs observed in the terrestrial planets' mantles.

The Earth-Moon system provides a particularly sensitive test for models of late accretion, given both experienced early global differentiation (Kleine et al., 2005; Boyet & Carlson, 2005), and shared a common impact bombardment. A consistent explanation for both the Earth, and Moon's HSE inventories remains enigmatic however, given that lunar HSEs are found in chondritic relative proportions, but with a concentration $20-40$ times lower than estimates for the terrestrial mantle (Day et al., 2007; Day & Walker, 2015). Most straightforwardly, this concentration would imply that total mass accretion to the Earth was three orders of magnitude greater than to the Moon, a discrepancy that cannot be attributed solely to the larger geometric cross section of the Earth (e.g., Walker, 2009).

Several quite different explanations have been subsequently proposed for this dearth of lunar HSEs. Bottke et al. (2010) first suggested the majority of Earth's HSEs were delivered by several large ($D > 2000\,\mathrm{km}$), leftover planetesimals from a population dominated by large objects. These large bodies would be more likely to be accreted by the Earth given its larger (gravitationally enhanced) accretional cross section, thus explaining the large discrepancy in Earth-Moon HSE abundances. This was supported on dynamical grounds by Raymond et al. (2013), who showed that by assuming a low initial angular momentum deficit, a late veneer dominated by large bodies could reproduce both Earth's late accreted mass, and the current-day orbital excitation of the terrestrial planets. Not only this, but the large Earth-Moon HSE abundance ratio could also be accounted for, given that the erosional nature of large impacts on the Moon naturally prevents the accretion of large ($> 500\,\mathrm{km}$) bodies (Raymond et al., 2013). Later work suggested that Earth's HSEs might instead have been delivered by a single lunar-sized impactor, rather than multiple Ceres-sized objects (Brasser et al., 2016).

Alternatively, Schlichting et al. (2012) proposed a late veneer of very small ($\sim 10\,\mathrm{m}$) planetesimals, which are collisionally damped to very low eccentricities, thereby increasing the relative gravitational focussing ratio in favour of the Earth. These planetesimals, assumed to form small (e.g., Weidenschilling, 2011), would naturally explain the damping of the terrestrial planets' eccentricities and inclinations following giant impacts. However, the extent to which such a population of small planetesimals could remain on near-circular orbits and avoid re-excitation by the terrestrial planets is unclear, and there is no alternative evidence supporting such a collisionally damped disk in the inner Solar System.

These studies all assume that HSEs are only removed from planetary mantles during core formation, and that their present abundances reliably trace subsequent mass accretion. Estimates of total mass accretion during the late veneer therefore strongly depend on this assumption. HSEs can, however, be removed from the mantle post-core formation; for example, the significant re-melting of the upper mantle during large impacts (e.g., Nakajima et al., 2021) has the capacity to strip extant HSEs delivered by previous (smaller) impactors.

The assumption that mantle HSE abundances reliably trace total mass accretion appears, however, questionable from a mineral physics perspective. Rubie et al. (2016) highlighted that HSEs could be removed from the mantle via the exsolution, and segregation of iron sulfide, which may occur during the crystallization of planetary magma oceans. Rubie et al. (2016) therefore proposed the alternative interpretation that HSEs only record mass accretion post-magma ocean crystallisation, which may occur much later than the initial stage of core-mantle differentiation. This would have significant consequences for the Earth-Moon system, given the lunar magma ocean may have crystallised up to 200 Myr after the Earth's, due to the rapid formation of an insulating anorthositic crust (Elkins-Tanton, 2008; Elkins-Tanton et al., 2011). While recent work suggests it unlikely that the lunar (or terrestrial) magma ocean reached sulfur saturation (Steenstra et al., 2020; Blanchard et al., 2025), both delayed lunar core formation (Day et al., 2021a), and tidally driven remelting of the lunar mantle (Nimmo et al., 2024) would similarly strip extant HSEs from the lunar mantle. It is therefore possible, given the steep decline in impact rate at early times, that the Moon accreted significantly more mass than appears to be recorded by its HSE record (Morbidelli et al., 2018).

The assumption that all delivered HSEs remain in Earth's mantle is also questionable from a geodynamical perspective. This is particularly problematic if the majority of mass accreted during the late veneer was delivered by large, differentiated planetesimals (e.g., Bottke et al., 2010; Brasser et al., 2016; Morbidelli et al., 2018). With the metallic core of such a differentiated planetesimal twice as dense as the silicate mantle, a significant fraction of this metal will likely sink through the mantle under the action of gravity, and eventually merge with Earth's core (e.g., Rubie et al., 2003; Deguen et al., 2014; Clesi et al., 2020). Thus, a significant fraction of this metal will be lost to the core without contributing to the mantle HSE signature of an impact (e.g., Marchi et al., 2018). Estimates of total mass accretion during the late veneer therefore depend crucially on the size distribution of leftover planetesimals, and the corresponding geodynamical processes controlling the efficiency of HSE delivery to the mantle (see figure 1).

The late accretion of large, differentiated planetesimals might therefore appear to be an inefficient mechanism for delivering metals to Earth's mantle. This is, however, in tension with strong chemical and isotopic constraints, which support the addition of impactor core material to Earth's mantle (Kleine et al., 2009; Dahl & Stevenson, 2010). Several recent studies have investigated the fate of impactor core material using both SPH and hydrocode simulations, all finding significant mass loss to Earth's core (e.g., Genda et al., 2017; Marchi et al., 2018; Citron & Stewart, 2022; Itcovitz et al., 2024). The proposed mechanisms of HSE delivery to the mantle however differ, and include the elongation and disruption of lunar-sized embryos (Genda et al., 2017), rapid three-phase flow at the base of an impact-generated magma ocean (Korenaga & Marchi, 2023), and the vaporisation of impactor core material (Albarède et al., 2013; Kraus et al., 2015; Itcovitz et al., 2024). Many important processes, dictating the fate of impactor core material, remain however on length scales far below simulation resolution. This is particularly challenging for many sources of turbulence, given that responsible instabilities are unable to propagate onto length scales that can be resolved (e.g., Dahl & Stevenson, 2010; Deguen et al., 2014). Accordingly, it is very challenging to accurately constrain the extent of mass loss to Earth's core.

In this study we combine both geophysical and astrophysical arguments to constrain the origin of Earth's mantle HSEs, and demonstrate that there is a contradiction between the observed concentrations of HSEs in the mantle, the geodynamics of HSE delivery, and current estimates of total mass accretion during the late veneer. In §2 we motivate the size-dependence of efficient HSE delivery, and determine a critical impactor size below which HSEs are efficiently entrained in the mantle. We present an analytical discussion of the buoyancy of metallic iron in both an impact-generated magma pond and a solid mantle, demonstrating that HSEs from impactors larger than approximately 1 km

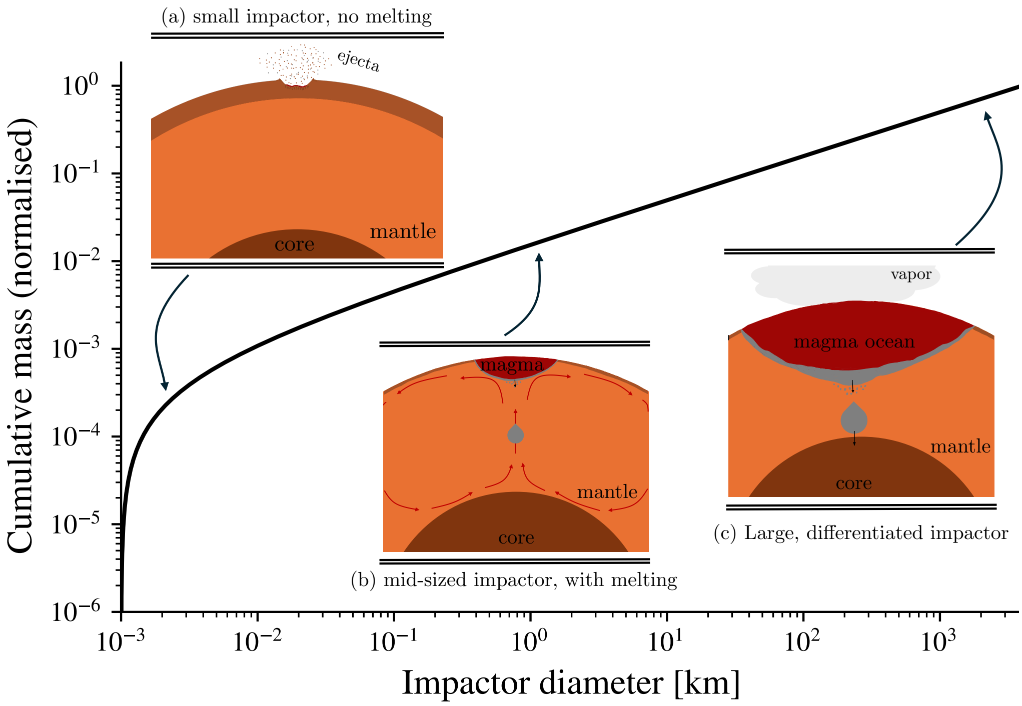

Figure 1. Collisions between leftover planetesimals drives the redistribution of mass between bodies of different sizes, generating a so-called collisional size-frequency distribution (SFD) dominated, in number, by the smallest bodies. The Earth will therefore, unavoidably, accrete planetesimals of a wide range of sizes during the late veneer. For the canonical collisional SFD (Dohnanyi, 1969), total mass is concentrated in the largest planetesimals (plotted above). The geodynamical processes responsible for the delivery of HSEs to the mantle, are controlled, primarily, by the size of the impactor, and therefore have the capacity to dramatically bias estimates of total mass accretion during the late veneer. We identify three possible regimes of HSE delivery, with illustrative schematic diagrams inset above. (a) Small impactors at low velocity will generate little melt, and are expected to fragment into millimetric pieces (see §2.1). The ability of these impactors to affect mantle geochemistry will depend on whether the tectonic regime of the planet enables them to be recycled into the mantle. (b) Small impactors at high velocity will generate significant melt, from both the target and impactor (Melosh, 1989). We expect metal diapirs to quickly enter the solid mantle (§2.2), bringing with them the impactor's HSEs. The ability of these impactors to affect mantle geochemistry will depend on whether the frictional force resisting diapir descent is larger than the negative buoyancy. (c) Large, differentiated impactors will generate large volumes of melt. Unless impactor core material can be fragmented into very small droplets, large diapirs will enter the solid mantle, and quickly sink to Earth's core (§2.3).

will be lost to Earth's core. We investigate in §3 the ability of small impactors to deliver observed HSEs, calculating the total mass accretion from larger bodies in an asteroid-like size distribution. In §4 we discuss the implications of this study for HSE delivery to the Earth and Moon, and for estimates of total mass accretion during the late veneer.

2 The entrainment of metal and its HSEs in the mantle

In this section, we demonstrate the importance of impactor size in determining the fate of its HSEs. In §2.1 we discuss the fate of an impactor's metal, and its HSEs, in the immediate aftermath of an impact. We then discuss the post-impact dynamics, as the impactor's metal experiences a negative buoyancy force in an impact-generated magma pond (§2.2), and a solid mantle (§2.3). From these discussions, we determine the critical impactor diameter above which an impactor's HSEs are lost to the core, and do not contribute to observed mantle HSE signatures.

2.1 The dispersal of metal and HSEs in the aftermath of an impact

Immediately after the Moon-forming impact, Earth's mantle will have been predominantly (if not fully) molten (e.g., Canup, 2008; Nakajima & Stevenson, 2015; Lock et al., 2018). Unlikely to have formed an insulating, conductive lid (Elkins-Tanton, 2008), mantle solidification will have been regulated by the transfer of heat through Earth's primitive atmosphere, occurring within $\sim 5\,\mathrm{Myr}$ of Moon-formation (Elkins-Tanton, 2008; Hamano et al., 2013). While the duration of late accretion remains uncertain, dynamical models suggest that the depletion timescale of leftover planetesimals was an order of magnitude larger (Morbidelli et al., 2018; Brasser et al., 2020). We therefore assume throughout that Earth's mantle had solidified post-Moon formation.

The ability of an impactor to contribute to mantle HSEs will depend on the spatial distribution of the impactor's metals immediately after an impact. This, in turn, is largely controlled by the impactor's initial structure (i.e., whether or not it is differentiated), its fate during collision with the Earth, and its ability to reach and melt the Earth's mantle. This last point is of particular importance, given that the geodynamics of metal descent through Earth's mantle depends sensitively on mantle viscosity (Dahl & Stevenson, 2010; Samuel, 2012). Since the viscosity of impact-generated melt will be more than 10 orders of magnitude smaller than the solid (crystallized) mantle below (V. Solomatov, 2015), the impact-driven melting of Earth's mantle is expected to play a central role in controlling the efficiency of HSE delivery.

We therefore anticipate a large diversity of post-impact scenarios (see figure 1), with substantially different consequences for the partitioning of HSEs between the mantle and core. We expect this diversity is largely driven by the impactor's size, as this predominantly controls the specific impact energy. This is illustrated most clearly through comparison of small impactors (figure 1a), which will generate little melt and remain embedded in the Earth's crust, and large differentiated impactors (figure 1c), which will generate significant silicate melt extending into the convective mantle. We discuss these end-member scenarios first, before addressing the transition (at intermediate sizes) between the efficient and inefficient delivery of HSEs to the mantle.

Evidence from terrestrial impact craters, which record little melting of the target, indicate that small impactors are fragmented into millimetric pieces during collisions with the Earth (Blau et al., 1973; Melosh & Collins, 2005; Folco et al., 2022), which may be subsequently oxidised by Earth's hydrosphere. The ability of small impactors to contribute to mantle geochemistry is therefore entirely reliant on the recycling of Earth's early crust. While there is debate regarding the Hadean Earth's tectonic regime, it is very likely that this early crust was recycled relatively quickly during the late veneer (e.g., Rosas & Korenaga, 2018). We will later demonstrate, in §2.3, that these millimetric fragments are small enough to remain in the solid target, and thus small impactors are able to efficiently contribute to Earth's HSEs, albeit over geologic timescales.

In contrast, the impacts of large differentiated bodies are violent events, which will readily break through the crust, melt the outer part of the mantle, and generate large volumes of silicate melt (Tonks & Melosh, 1993; Nakajima et al., 2021). The impact-generated shock wave will similarly melt the impactor, such that its metallic liquid core is released into the magma pond; these metal droplets are more than twice as dense as the surrounding molten silicates, and are thus liable to quickly sink, and collect at the bottom of the newly-formed magma pond (Deguen et al., 2014). The geodynamics of this process, and the subsequent fate of metals as they enter the convective mantle are therefore crucial to an impactor's ability to contribute to mantle geochemistry. This is discussed next, in §2.2 and §2.3, in which we demonstrate that a significant fraction of impactor core material will be lost to Earth's core.

We therefore anticipate that there must exist a critical impactor diameter, D_{crit}, which delineates the transition between the fragmentation of smaller impactors (which will distribute their HSEs throughout the Earth's crust), and the generation of significant melt during much larger impacts (with their metals subsequently liable to gravitational instability, and loss to Earth's core). In the following paragraphs, we estimate the value of this critical, intermediate, impactor diameter, D_{crit}.

Through comparison of the above end-member scenarios, it is apparent that the extent of melting during an impact is fundamentally important in determining the post-impact fate of metals. Previous studies have demonstrated that the amount of impact-generated melt depends on both the impact velocity and angle (e.g., Pierazzo et al., 1997), which determine the peak shock pressure experienced during compression. However, this is very complex for oblique impacts (Pierazzo & Melosh, 2000). Using the results from Potter and Collins (2013), who studied this in detail, we find the critical impact velocity for the significant melting of impactor material is in the range $12-15\,\mathrm{km\,s^{-1}}$ (see Appendix A). Such high velocity impacts will concurrently generate significant melting of the target, which requires $v_{\mathrm{imp}}^2/E_m \gtrsim 30$, where E_m is the internal energy of melting (Pierazzo et al., 1997).

The impact velocity of small bodies at Earth's surface, v_{imp}, depends on both the entry speed of an impactor (which will always exceed $11.2\,\mathrm{km\,s^{-1}}$), and its interaction with the atmosphere. The significance of this interaction, dominated by atmospheric deceleration and fragmentation, is largely governed by the impactor's size (with large bodies able to reach the surface almost unperturbed), and the surface density of Earth's early atmosphere (e.g., Chyba et al., 1993; Svetsov et al., 1995; Melosh & Collins, 2005). The evolution of Earth's atmosphere remains subject to debate, particularly during the Hadean, but is thought to have been initially very dense ($\sim 100\,\mathrm{bar}$), following the degassing of Earth's magma ocean (Elkins-Tanton, 2008). A relatively quick transition in atmospheric pressure is then expected, which by the end of the Hadean is inferred to be less than 1 bar (Rimmer et al., 2019; Catling & Zahnle, 2020). Using the simple atmospheric entry model from Chyba et al. (1993), we find the critical diameter for melting thus varies in the range $\sim 10-1000\,\mathrm{m}$ (see figure A2), corresponding to the plausible variation in atmospheric surface pressure during the Hadean (see Appendix A for more detailed discussion of this model). Smaller impactors will be unable to reach the surface intact, or at a sufficiently high velocity as required to melt both impactor and target material. This suggests the critical diameter, D_{crit}, is at most on the order of 1 km.

Another important consideration, that is likely to inform the value of the critical diameter D_{crit}, is the ability of an impactor to reach the convective mantle. When the impactor's metal is directly implanted into the convective mantle, it will immediately sink due to its density difference with the surrounding silicates, and can be potentially lost to the core (figure 1). In contrast, metals injected into the crust will remain trapped there until admixed into the mantle. In the latter scenario, metals may be oxidised before reaching the mantle, and hence may contribute to observed HSE signatures. The minimum impactor size required to penetrate Earth's crust can be estimated using scaling laws for impact crater depths. Using the crater depth scaling from Allibert et al. (2023), we find that for a 1 km diameter impactor (assuming a typical impact velocity of $20\,\mathrm{km\,s^{-1}}$), crater depths exceed 10 km, which is sufficient to penetrate modern oceanic crust. Whilst the thickness of Earth's early crust is uncertain and subject to significant debate (Korenaga, 2018), it was likely much thinner than of the modern Earth. It therefore appears overwhelmingly likely that impactors larger than 1 km would penetrate Earth's early crust.

Given the consensus between these two independent lines of investigation, we therefore suggest that $D_{\mathrm{crit}} \sim 1\,\mathrm{km}$ marks an important transition in the post-impact fate of HSEs; smaller bodies will fragment into small pieces, distributing their HSEs throughout Earth's crust, whereas larger bodies will simultaneously penetrate the crust, and generate significant melt. The true fate of HSEs will of course be the result of many physical processes spanning a wide range of length scales; we therefore stress there remains uncertainty in this critical impactor size, which we revisit in §4.3. Next, we focus on the fate of larger impactors ($D > 1\,\mathrm{km}$), first investigating the fate of metals in a magma pond (§2.2), and then the solid mantle (§2.3).

2.2 The entrainment of metal in a magma pond

During collision with Earth, high-resolution simulations (e.g., Kendall & Melosh, 2016) observe the stretching of an impactor's metallic core, which is spread into a thin layer over the crater floor. This metal is stretched further during the formation of a strong, vertical jet during crater collapse, fragmenting $\sim 100\,\mathrm{km}$ cores into km-scale 'blobs' (Kendall & Melosh, 2016) – the resolution limit of these simulations. Analogue experiments reveal that turbulent mixing drives further metal fragmentation down to the capillary scale, forming small droplets stabilized via surface tension (Deguen et al., 2014; Wacheul & Le Bars, 2018; Landeau et al., 2021; Maller et al., 2024). Despite the fast equilibration expected between these small metal droplets and the silicate melt (Ulvrová et al., 2011; Lherm & Deguen, 2018; Clesi et al., 2020), we expect there will be no significant flux of elements between these phases given the large metal-silicate partition coefficients of the HSEs (Righter et al., 2008; Mann et al., 2012). Hence, we restrict our attention to the entrainment of impactor metal, and its HSEs, in the newly-formed magma pond.

We assume that the impactor's metal core fragments into drops of diameter d and density ρ_m, which settle in a fully liquid silicate magma pond of viscosity μ_s, density ρ_s, and depth H, convecting turbulently at velocity U. Particles can be suspended in a convective layer when the frictional force is large enough relative to the buoyancy force of each particle (V. S. Solomatov et al., 1993; Sturtz et al., 2021; Monteux et al., 2023). The Shields number

$$\theta_S = \frac{\tau}{\Delta\rho\, g\, d}, \tag{1}$$

compares these two forces, where τ is the shear stress induced by the convection, $\Delta\rho = \rho_m - \rho_s$ the density difference, and g the gravitational acceleration.

Previous studies have shown that there exists a critical value, above which particles can be re-entrained by convective motions, which is given by $\theta_c = 0.15 \pm 0.05$ (V. S. Solomatov et al., 1993; Sturtz et al., 2021; Monteux et al., 2023). Drops with $\theta_S < \theta_c$ will always sediment out of the convecting layer. While this condition has only been tested for solid particles, we expect that the additional stabilising force provided by surface tension will make the entrainment of liquid drops even more challenging.

In a fully liquid magma pond with a depth, H, of $\sim 1000\,\mathrm{km}$, convective speeds are typically on the order of $10\,\mathrm{m\,s^{-1}}$ (V. Solomatov, 2015). With a low viscosity on the order of $0.05\,\mathrm{Pa\,s}$ (Karki & Stixrude, 2010), the Reynolds number, which measures the ra-

Parameter Unit	$g_\oplus$ $\mathrm{m\,s^{-2}}$	g_L $\mathrm{m\,s^{-2}}$	α [a] $\mathrm{K^{-1}}$	ρ_s [b] $\mathrm{kg\,m^{-3}}$	ρ_m [c] $\mathrm{kg\,m^{-3}}$	C_p [d] $\mathrm{J\,kg^{-1}}$	k_s [e] $\mathrm{m^2\,s^{-1}}$
Value	9.8	1.62	3×10^{-5}	4500	9000	10^3	10^6

Table 1. Assumed mantle and metal properties used in sections 2.2 and 2.3. Values are compatible with published studies: [a] (Chopelas & Boehler, 1992), [b] (Miller et al., 1991), [c] (Morard et al., 2013), [d] (Stebbins et al., 1984), [e] (de Koker, 2010).

Parameter Unit	ΔT K	H m	U $\mathrm{m\,s^{-1}}$	F $\mathrm{W\,m^{-2}}$	μ_s Pa s
Value	$500-2500$	$10^6-3\times10^6$	$4-40$	$3\times10^5-10^6$	$0.02-0.08$

Table 2. Ranges of plausible parameter values relevant for a fully liquid magma ocean. Ranges for ΔT, H and U are from (V. S. Solomatov, 2000), the viscosity range from (Karki & Stixrude, 2010) and the range of possible heat flux F from several studies (V. Solomatov, 2015; Lebrun et al., 2013).

tio of inertia to viscous forces, is larger than 10^{11}, meaning that the flow is fully turbulent (Salvador & Samuel, 2023). In such a turbulent magma pond, the largest shear stresses are likely the Reynolds stresses (V. S. Solomatov et al., 1993; V. Solomatov, 2015),

$$\tau = \rho_s\, u^2, \tag{2}$$

where u is the friction velocity (Shraiman & Siggia, 1990),

$$u = \frac{U}{x}, \tag{3}$$

and x satisfies

$$x = 2.5\,\log\left(\frac{\rho_s\,U\,H}{\mu_s}\frac{1}{x}\right) + 6. \tag{4}$$

We assume that the convective velocity U follows the scaling for hard turbulence (Shraiman & Siggia, 1990; V. Solomatov, 2015)

$$U = 0.086\,x\,\left(\frac{\alpha\,g\,H\,F}{\rho_s\,C_p}\right)^{1/3}, \tag{5}$$

where α is the thermal expansion coefficient, F the heat flux at the top of the magma pond, and C_p the specific heat capacity under constant pressure. Using the typical values for U, μ_s, and H in a deep magma ocean (Tables 1 and 2), one finds that x is in the range $60-75$, and the friction speed is typically in the range $0.1-0.5\,\mathrm{m\,s^{-1}}$.

Inserting (2) into the definition of the Shields number (1), one finds that the condition $\theta_S > \theta_c$ is met when the drop diameter is smaller than

$$d_{\text{entr.}} = \frac{\rho_s\,u^2}{\theta_c\,\Delta\rho\,g}. \tag{6}$$

With a friction speed of about $0.1{-}0.5\,\mathrm{m\,s^{-1}}$, the critical diameter $d_{\text{entr.}}$ for entrainment is on the order of $1{-}10$ cm; drops smaller than 1 cm may therefore be entrained by the convection. This critical drop size is for a deep magma pond on the order of 1000 km. In shallower magma ponds, the convective velocity (equation 5), the friction speed (equation 4), and hence the Reynolds stresses (equation 2) are lower, making the entrainment

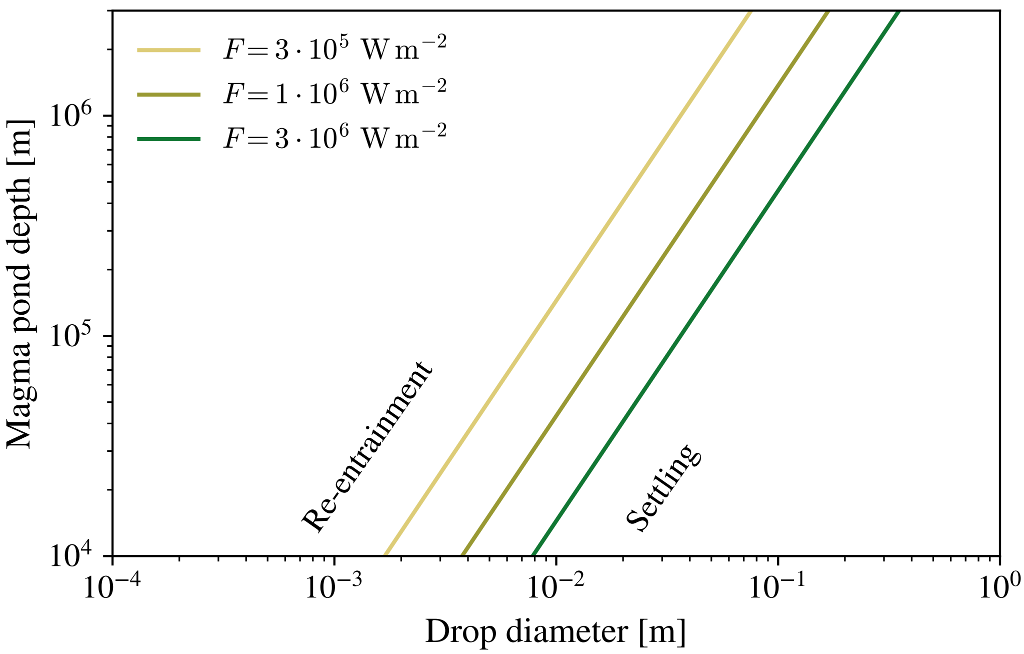

Figure 2. The maximum diameter of metal drops that can be entrained by turbulent convection in a fully liquid magma pond, $d_{\mathrm{entr.}}$ (corresponding to the condition $\theta_S = \theta_c$; equation 6), as a function of magma pond depth for three plausible values of the heat flux F. The friction speed u in equation (6) is computed from equations 3-5. Note that $\theta_S = \theta_c$ is a necessary, not sufficient condition for entrainment, and so metal drops smaller than this maximum diameter will not all remain suspended in equilibrium (see equation 7, figure 3).

of metal drops significantly harder. This is shown in figure 2, where we observe that the maximum drop diameter for entrainment decreases as the magma pond depth decreases.

The diameter d of metal drops in magma oceans remains poorly known. Yet, previous studies have obtained orders of magnitude estimates for the drop size when metal fragments after a large planetary impact (Deguen et al., 2014). Using existing theories for fragmentation in a turbulent flow (Hinze, 1955), they obtain $d \sim 1$ mm (Deguen et al., 2014). More recent experiments on the impact of a liquid onto an immiscible liquid bath also suggest that the impactor core fragments into drops of 0.3 mm in Earth's magma ocean (Maller et al., 2024). Because these drops are smaller than $d_{\mathrm{entr.}} \sim 1$ cm, they will not necessarily sediment directly out of the convecting layer.

The condition $\theta_S > \theta_c$ is, however, a necessary, but not sufficient condition for the entrainment of metal drops. When $\theta_S > \theta_c$, drops will constantly sediment out of the convective region, whilst others are re-entrained by the convective motions (V. S. Solomatov et al., 1993). When the flux of settling drops balances the flux of re-entrained ones, the mass of suspended drops reaches an equilibrium. The mass of drops kept in suspension is then dictated by an energy balance (V. S. Solomatov & Stevenson, 1993). Indeed, only a fraction ϵ of the energy generated by buoyancy forces is converted into the gravitational energy of the dense, suspended metal drops. The suspended (volume) fraction of metal drops, at equilibrium, then reads (V. S. Solomatov & Stevenson, 1993),

$$\Phi = \epsilon \frac{\alpha F}{C_p \, \Delta\rho \, U_d} \tag{7}$$

where ϵ is an empirical, dimensionless efficiency factor that varies in the range 0.2%–0.9% (V. S. Solomatov et al., 1993; Lavorel & Le Bars, 2009), U_d the settling speed of an individual drop.

We assume that the settling speed is given by,

$$U_d = \sqrt{\frac{4\,\Delta\rho\, g\, d}{3\,\rho_s\, C_d}}, \tag{8}$$

where C_d is the drag coefficient. The value of C_d depends on the drop Reynolds number $Re_d = \rho_s\, U_d\, D/\mu_s$, which measures the relative importance of inertial and viscous forces around the drop. The value of Re_d is typically lower than 1 for metal drops with a diameter $d \lesssim 10^{-4}$ m but it reaches 10^3 for larger drops with $d = 1\,\mathrm{cm}$. In this range of Re_d, the settling velocity U_d varies from the Stokes regime, when $Re_d < 1$, to a regime of nearly constant drag coefficient. To describe this transition we use the empirical model proposed by (Samuel, 2012) in which

$$C_d = \frac{24}{Re_d} + c_N, \tag{9}$$

where $c_N = 0.3$, $Re_d = \rho_s\, U_{d,S}\, d/\mu_s$ and

$$U_{d,S} = \frac{g\,\Delta\rho d^2}{18\,\mu_s} \tag{10}$$

is the Stokes velocity.

With this choice, when $Re_d \ll 1$, $C_d \simeq 24/Re_{d,S}$ and U_d from (8) tends to the Stokes velocity (10), which increases as the square of the drop diameter. Instead, in the limit of large Re_d, C_d tends to the value $c_N = 0.3$, meaning that U_d increases as the square root of the drop diameter.

Inserting equations (8), (9), and (10) into equation (7), one obtains the volume fraction Φ of entrained metal as a function of the drop diameter d. In all regimes, the larger the drops, the larger the settling speed U_d, and hence, the lower the fraction of entrained metal Φ. This suspended fraction is shown in figure 3 as a function of the drop diameter d for an Earth-like planet with a deep magma ocean, and for different values of the heat flux F. In a fully liquid magma pond, with viscosity $\lesssim 0.1\,\mathrm{Pa\,s}$, 1D convective thermal evolution models predict a surface heat flux in the range $3{\times}10^5{-}10^6\,\mathrm{W\,m^{-2}}$ (V. S. Solomatov, 2000; Lebrun et al., 2013; Salvador et al., 2017). To be conservative, we explore the larger range $3 \times 10^5 - 3 \times 10^6\,\mathrm{W\,m^{-2}}$.

Assuming millimetric metal drops, the volume fraction of suspended metal is more than three orders of magnitude smaller than required to account for observed HSEs in Earth's mantle (figure 3). We predict that, to keep enough metal in suspension and match HSE concentrations in Earth's mantle, the metal drops need to be smaller than $3{\times}10^{-5}\,\mathrm{m}$ with $F = 10^6\,\mathrm{W\,m^{-2}}$ (figure 3). Even with an extreme heat flux of $3{\times}10^6\,\mathrm{W\,m^{-2}}$, drops need to be smaller than $5{\times}10^{-5}\,\mathrm{m}$. This is more than one order of magnitude smaller than the mean drop size expected after an impact ($\sim 1\,\mathrm{mm}$; Deguen et al., 2014; Wacheul & Le Bars, 2018; Maller et al., 2024). While there will be a distribution of drops below this size, much of the mass expected to be in the largest drops. There will therefore be insufficient mass in small drops to account for Earth's HSEs (see Appendix B).

We expect this critical drop size to be independent of the depth of the magma pond (H), given that the suspended metal fraction is proportional to the heat flux at the surface of the magma pond ($F \propto Ra^{1/3}/H$), which is itself independent of H given that the Rayleigh number scales as $Ra \propto H^3$. We further note that the suspended metal fraction changes insignificantly if we assume a lower density $\rho_m \approx 7800\,\mathrm{kg\,m^{-3}}$, as may be appropriate for smaller magma ponds. Unless additional fragmentation mechanisms

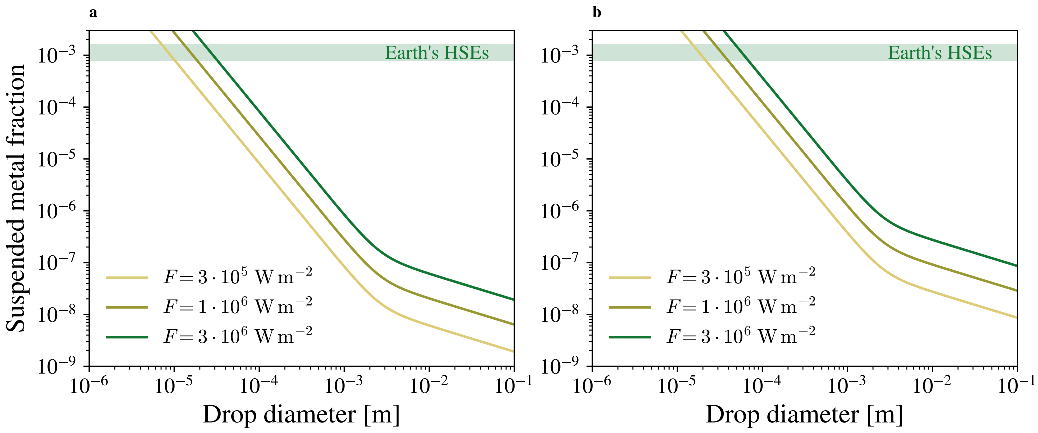

Figure 3. Volume fraction of suspended metal in a turbulent magma ocean on an Earth-sized planet as a function of the metal drop diameter, for three plausible values of the heat flux F. The green shaded band locates the suspended volume fraction needed so that the HSE concentration in the magma pond matches that of the present-day Earth's mantle. We use equations 7-10 assuming $g = 9.8\,\mathrm{m\,s^{-2}}$, $\rho_m = 9000\,\mathrm{kg\,m^{-3}}$, $\rho_s = 4500\,\mathrm{kg\,m^{-3}}$, $\mu_s = 0.05\,\mathrm{Pa\,s}$ and $H = 2000\,\mathrm{km}$. (a) Lower-end estimates assume $\epsilon = 0.2\%$. (b) Upper-end estimates with $\epsilon = 0.9\%$.

generate drops smaller than 0.05 mm, we therefore expect metal (from molten impactors) to rapidly settle and coalesce into a layer at the bottom of the newly-formed magma pond. In §2.3 we consider the stability of these metal pools (which overlay a layer of solid, or partially solid mantle; see figure 1b), and the subsequent fate of impactors' HSEs.

2.3 The entrainment of metal diapirs in the mantle

Here, we consider that the boundary between the liquid and solid mantle is defined by the fraction of silicate crystals; when this fraction exceeds $\sim 60\%$, the viscosity increases by orders of magnitude and the convective dynamics switches from turbulent to laminar (Lejeune & Richet, 1995; V. S. Solomatov, 2000; Costa, 2005). Thick metal ponds that accumulate at this rheological boundary are subject to Rayleigh-Taylor instabilities (Karato & Rama Murthy, 1997). These instabilities form large metal diapirs that are comparable in size to the metal pond they originate from (Karato & Rama Murthy, 1997; Fleck et al., 2018; Olson & Weeraratne, 2008). We therefore consider a metal diapir of diameter d, which is on the same order as the impactor core diameter, settling in a solid, or partially solid mantle (see figure 1b). The diapir's exact size will depend on the impactor's metal content (i.e., Fe-Ni mass fraction), which for ordinary and enstatite chondrites varies in the approximate range $f_{\mathrm{met}} \sim 5\text{–}30\,\%$ (e.g., Scott & Krot, 2003). The diapir will thus be a fraction $(f_{\mathrm{met}}\rho_{\mathrm{c}}/\rho_{\mathrm{FeNi}})^{1/3} \sim 0.3\text{–}0.5$ of the impactor's diameter.

As in the magma ocean, these diapirs are re-entrained by convection only when the Shields number θ_S (equation 1) exceeds $\theta_c = 0.15 \pm 0.05$ (V. S. Solomatov et al., 1993; Sturtz et al., 2021; Monteux et al., 2023). However, in a high-viscosity laminar mantle, the shear stresses are now proportional to the convective speed (V. S. Solomatov et al., 1993),

$$\tau \propto \frac{\mu_s U}{H}. \tag{11}$$

We expect the kinematic viscosity of a solid or partially solid mantle to be in the range $\nu_s \sim 10^{13} - 10^{15}\,\mathrm{m^2\,s^{-1}}$ (Ita & Cohen, 1998; V. S. Solomatov, 2000; V. Solomatov, 2015), and the thermal diffusivity of the order $k_s \sim 10^{-6}\,\mathrm{m^2\,s^{-1}}$ (Freitas et al., 2021). These values are more than nineteen orders of magnitude apart, such that momentum diffusivity will dominate energy transfer, and the Prandtl number $Pr = \nu_s/k_s$ can be considered infinite.

We assume stress-free boundary conditions at the top and bottom of the mantle, given both the top layer (the liquid magma ocean) and bottom layer (the liquid outer core) have viscosities orders of magnitude smaller than the partially solid mantle. In this limit of infinite Prandtl number, and with stress-free boundary conditions, the typical convective velocity U satisfies the following scaling,

$$U = c\frac{k_s}{H}Ra^{2/3}, \tag{12}$$

where $Ra = \alpha g \Delta T H^3/k\nu$ is the Rayleigh number, α the thermal expansion coefficient, and ΔT the temperature difference across the mantle. In previous experimental and numerical studies, the coefficient c has been found to vary in the range $\sim$0.05-0.2 (Jarvis & Peltier, 1982; Turcotte & Schubert, 2002; Agrusta et al., 2020). Combining equations (1) and (12), we obtain the critical diapir size that a convecting mantle can potentially sustain,

$$d_{\mathrm{entr.}} = c\frac{\left(k_s\,\mu_s\,\rho_s^2\,\alpha^2\,\Delta T^2\right)^{1/3}}{\Delta\rho\,\theta_c\,g^{1/3}}. \tag{13}$$

This critical diapir size, shown in figure 4, is most sensitive to uncertainties in the mantle viscosity, which is expected to depend strongly on depth and viscosity (e.g., Ita & Cohen, 1998; V. S. Solomatov, 2000). Considering mantle viscosities in the range 10^{16}–10^{19} Pa s (see Table 1 for the assumed mantle properties), this critical diapir size varies (approximately) in the range $1-100$ m. These estimates for the critical diapir size agree with those of Karato and Rama Murthy (1997). Larger diapirs will not be adequately supported by convective shear stresses, and will therefore sink quickly to Earth's core.

We stress that equation (13) is a local criterion, balancing shear stresses and the negative buoyancy of the diapir at a given depth in the mantle. When assuming a solidus temperature of about 3000 K at the top of the partially solid mantle (Andrault et al., 2011), temperature-dependent viscosity models (adopting parameters used previously in the literature for solid mantles and mushy magma oceans; e.g., Roberts & Zhong, 2006; Maurice et al., 2017) predict that a variation in temperature of about 1000 K throughout the partially solid mantle would cause the viscosity to vary within the range 10^{16}–10^{19} Pa s, compatible with the range considered in figure 4. We therefore expect this critical diapir size, of order $1-100$ m, to still hold when accounting for a temperature-dependent viscosity.

2.4 Summary: HSE delivery to the mantle depends on impactor size

We have demonstrated in §2.1 that impactors larger than $\sim$1 km will readily penetrate Earth's crust, and generate significant melt (from both the target, and impactor itself). After such impacts, the impactor's metals will fragment into small drops in the newly-formed magma pond. Given a typical drop size of 1 mm (Deguen et al., 2014; Maller et al., 2024), we demonstrated in §2.2 that the fraction of entrained metal would be two orders of magnitude smaller than is required to account for the observed concentration of HSEs in Earth's mantle (figure 3). These metals will therefore rapidly accumulate at the base of the magma pond, forming a layer unstable to Rayleigh-Taylor instabilities. Metal diapirs, of comparable size to the impactor, will subsequently migrate into the solid mantle. With typical size much larger than the critical diameter for convective entrain-

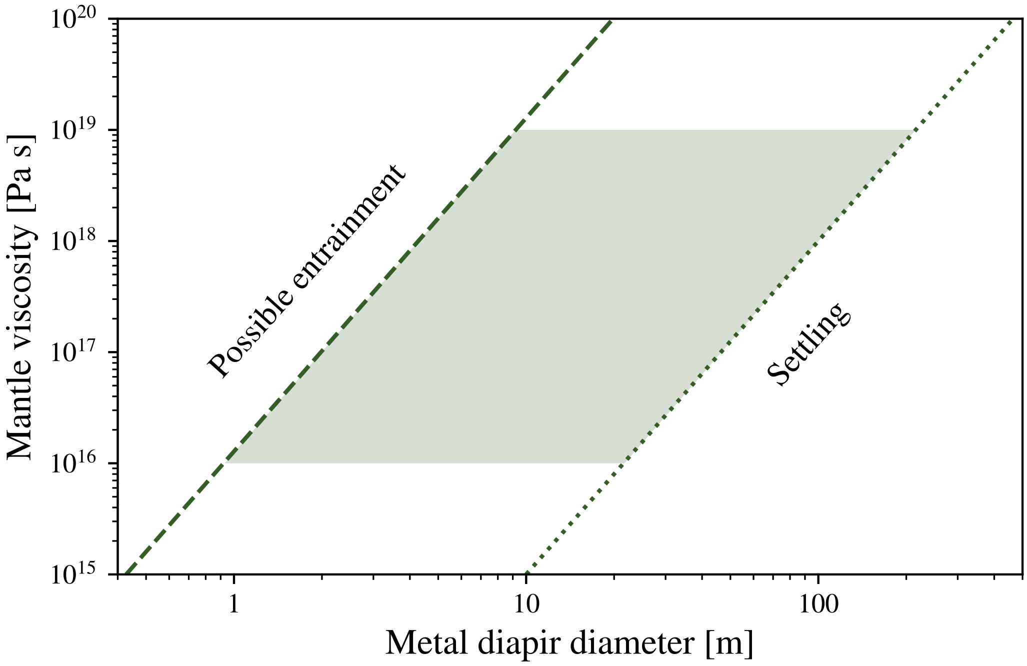

Figure 4. The maximum diameter of metal diapirs that can be entrained by mantle convection, $d_{\mathrm{entr.}}$ (equation 13), as a function of mantle viscosity. The dashed green line corresponds to the lower estimate, using $c = 0.05$, $\Delta T = 500\,\mathrm{K}$, $\theta_c = 0.4$, while the dotted green line shows the higher estimate, with $c = 0.02$, $\Delta T = 2500\,\mathrm{K}$, $\theta_c = 0.2$. The shaded region indicates typical values expected for a partially solid mantle on the early-Earth.

ment in the solid mantle ($\sim 1{-}100\,\mathrm{m}$; §2.3), these diapirs will be lost to Earth's core, leaving no HSE signature in the mantle. In contrast, evidence from terrestrial impact craters suggest that smaller impactors ($\lesssim 1\,\mathrm{km}$) are fragmented into millimetric pieces during impact (Blau et al., 1973; Melosh & Collins, 2005; Folco et al., 2022). Impactors smaller than 1 km should therefore efficiently contribute to mantle HSE signatures thanks to efficient crustal recycling on the early Earth.

The efficient delivery of HSEs to the mantle is thus strongly dependent on impactor size. Most strikingly, in the absence of some mechanism capable of disrupting core material into very small (i.e., $\lesssim 0.01\,\mathrm{mm}$) fragments in a magma pond, large differentiated planetesimals will be unable to account for Earth's mantle HSEs. These are commonly invoked as the source of Earth's HSEs (e.g,. Bottke et al., 2010; Brasser et al., 2016), and comprise the majority of the total mass in an asteroid-like size distribution (see figure 1). This therefore has significant implications for either the source of Earth's HSEs, or estimates of total mass accretion during the late veneer. We discuss this next.

3 HSE delivery via the entrainment of small impactors

Motivated by the results of the previous section, in which we demonstrated that metals from only impactors smaller than $\sim 1\,\mathrm{km}$ will be convectively entrained in Earth's mantle, we consider the feasibility of these impactors as the source of observed HSEs. In particular, we investigate the implications this would have for total mass accretion during the late veneer, and its consistency with the crucial, independent observational constraint on late accretion provided by the Moon.

A similar scenario was initially proposed by Schlichting et al. (2012), who invoked a late veneer sourced by a population of small ($\sim 10\,\mathrm{m}$) planetesimals. Schlichting et al. (2012) demonstrated that, by forming a collisionally damped disk, these planetesimals could effectively damp the eccentricities and inclinations of the terrestrial planets, whilst also increasing Earth's gravitational cross section relative to the Moon. This was suggested to provide a simple resolution for the high HSE ratio that is observed. A challenge for this scenario, however, is that it can only reproduce an Earth-Moon HSE ratio as high as 200, inconsistent with mantle abundances that indicate this ratio is closer to $\sim 2000-3000$ (Day & Walker, 2015). We note that Schlichting et al. (2012) identified the lunar crust as an additional HSE reservoir, which could prevent HSE delivery to the mantle, and thereby reduce the Earth-Moon HSE ratio. Few samples however, from both the lunar regolith and impact melt breccias, record sufficiently high HSE concentrations (Day & Walker, 2015; Day et al., 2016), suggesting the lunar crust did not provide such an effective barrier during the late veneer.

In this section we provide two further arguments against the delivery of HSEs via small planetesimals. Specifically, we show that in order to deliver sufficient mass in small bodies from an asteroid-like size distribution, an implausibly large mass must also be delivered in larger planetesimals, which would be lost to Earth's core. If, instead, there was a dearth of large planetesimals, HSEs would be delivered predominantly to the lunar crust, rather than the mantle, in tension with observational constraints (Ryder, 2002; Day & Walker, 2015).

3.1 Mass constraints: an accretion catastrophe

In the absence of alternative evidence supporting a (collisionally damped) disk of small planetesimals in the inner Solar System, we assume they are a subset of a larger population with a power-law size-frequency distribution (SFD),

$$n(D)dD = KD^{-\alpha}dD, \tag{14}$$

for $D \in [D_{\min}, D_{\max}]$, where D is the impactor diameter, α the slope of the distribution, and K a constant of proportionality. The assumption that it is only impactors with $D < D_{\mathrm{crit}}$ that deliver HSEs to the mantle allows us to constrain the constant of proportionality,

$$K = \left(\frac{6M_{\mathrm{HSE},\oplus}}{\pi\rho_{\mathrm{imp}}}\right)\left(\int_{D_{\min}}^{D_{\mathrm{crit}}} D^{3-\alpha}dD\right)^{-1}, \tag{15}$$

where ρ_{imp} is the characteristic impactor density. The Earth will unavoidably accrete excess mass, that will make no contribution to mantle HSE signatures, from impactors in the size range $[D_{\mathrm{crit}}, D_{\max}]$, with the total accreted mass given by

$$M_{\mathrm{acc,tot}} = \int_{D_{\min}}^{D_{\max}} \left(\frac{\pi\rho_{\mathrm{imp}}K}{6}\right) D^{3-\alpha}dD = M_{\mathrm{HSE},\oplus}\left(\frac{\int_{D_{\min}}^{D_{\max}} D^{3-\alpha}dD}{\int_{D_{\min}}^{D_{\mathrm{crit}}} D^{3-\alpha}dD}\right). \tag{16}$$

Total mass accretion during the late veneer quickly exceeds traditional estimates of 0.5 % (Day et al., 2007; Walker, 2009), as shown in figure 5. This is a consequence of the fact that the total mass in a collisional SFD is predominantly concentrated within the largest planetesimals (see figure 1). Assuming a critical diameter $D_{\mathrm{crit}} \sim 1\,\mathrm{km}$ (see §2), and a maximum impactor diameter $D_{\max} \sim 1000\,\mathrm{km}$ (as observed in the present-day asteroid belt), total mass accretion is in excess of 20 Moon masses ($\sim 25\,\%$ of Earth's mass). Figure 5 (a) demonstrates this mass accretion catastrophe is even more problematic (with total mass accretion approaching Earth's mass) when adopting estimates for the main asteroid belt's SFD, for which α is in the range [2.1, 3.3] for asteroids smaller than 100 km (e.g., Bottke et al., 2005; Gladman et al., 2009; Masiero et al., 2011), or assuming a SFD inherited from the streaming instability, which constrains α to the (shallower) range [1.9-2.8] (Johansen et al., 2015; Simon et al., 2016).

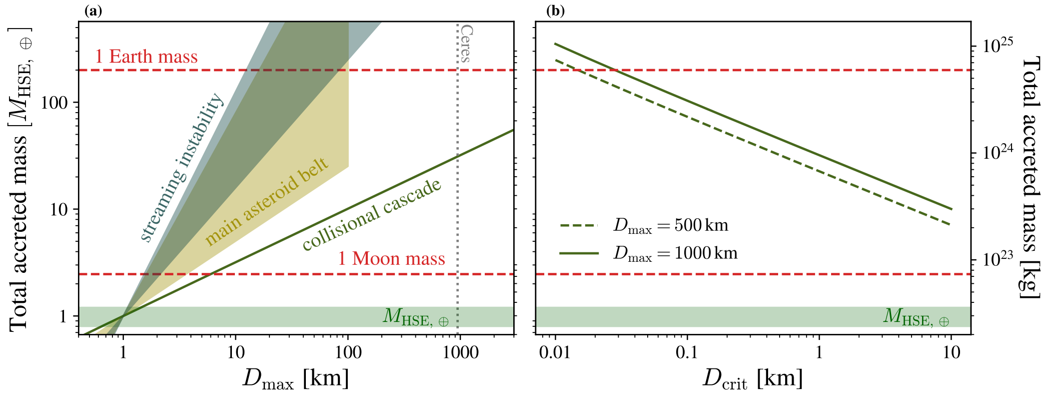

Figure 5. Total mass accretion to the Earth is calculated, assuming all observed HSEs ($M_{\mathrm{HSE},\oplus}$) are delivered by impactors smaller than D_{crit}, from a collisional size distribution ($n(D)dD \propto D^{-7/2}dD$; Dohnanyi, 1969) with maximum impactor diameter $D_{\max}$. (a) We vary $D_{\max}$, while keeping $D_{\mathrm{crit}} = 1$ km fixed, and find total mass accretion from larger bodies quickly becomes unrealistically large. Estimates for the main asteroid belt, and streaming instability are included for reference, in blue and yellow respectively, which deliver even more mass in $D > D_{\mathrm{crit}}$ impactors. (b) Total mass accretion is calculated as a function of D_{crit}, which is largely determined by the Earth's early-atmosphere (see Appendix A). Total mass accretion remains implausibly large in the presence of large (~ 500 km) planetesimals, as are found in present-day asteroid belt, and predicted by the streaming instability.

Total mass accretion to the Earth is therefore unrealistically large during the late veneer if all observed HSEs are delivered by small ($< D_{\mathrm{crit}}$) planetesimals. The delivery of HSEs via the direct, convective entrainment of small impactors therefore precludes the existence of any larger bodies in the impactors' size distribution, in clear tension with predictions from the streaming instability (Johansen et al., 2015; Simon et al., 2016). There remains debate however regarding the origin of the largest bodies in the MAB (Durda et al., 1998; Bottke et al., 2005; Morbidelli et al., 2009; Weidenschilling, 2011), such that it is impossible to preclude the possibility that there was a dearth of large planetesimals during the late veneer.

An impacting population consisting only of small planetesimals (e.g., Weidenschilling, 2011) would therefore seem the only way to avoid the mass-accretion catastrophe described in this section. As we show next, in §3.2, this would instead violate available constraints from the Moon's crust and mantle HSE budgets, thereby precluding the delivery of HSEs via small impactors.

3.2 HSEs from small impactors cannot reach the lunar mantle

Lunar mare basalts indicate the efficient mixing of HSEs into the lunar mantle from $\sim 1.5 \times 10^{19}$ kg of impactor material (Day et al., 2007; Day & Walker, 2015), whilst the lunar crust records the addition of only 0.5×10^{19} to 1.0×10^{19} kg of impactor material (Ryder, 2002; Day & Walker, 2015). As previously discussed, this leaves an order of magnitude discrepancy between the observed Earth-Moon HSE ratio, and what is possible via gravitational focussing. Some process capable of removing HSEs from the lunar mantle post core-formation (e.g., FeS exsolution, delayed lunar core formation, or tidal driven remelting; Rubie et al., 2016; Day et al., 2021b; Nimmo et al., 2024) is therefore required to match this important observational constraint. A direct consequence of this requirement is that HSEs currently observed in the lunar mantle were delivered post-magma ocean crystallisation. Small impactors must therefore be able to penetrate the thick lunar crust. We demonstrate here that this is very challenging, if not impossible, for small impactors.

In contrast to the rapid solidification of Earth's mantle (Elkins-Tanton, 2008; Hamano et al., 2013), the lunar mantle is expected to evolve slowly from its initially molten state post-formation. Samples from the lunar highlands first motivated the hypothesis that anorthite plagioclase was buoyantly segregated during magma ocean crystallisation, forming a thick anorthositic crust (e.g., Wood et al., 1970). Such an insulating lid was able to efficiently regulate the rate of cooling of the magma ocean, extending the timescale over which it solidified to $\sim 10-200\,\mathrm{Myr}$ (Elkins-Tanton et al., 2011). Given this timescale is comparable to that of the late veneer (Morbidelli et al., 2018; Brasser et al., 2020), it is likely that many impacts will have been onto a thick crust overlaying liquid magma (Jackson et al., 2023; Engels et al., 2024). While this represents a significant deviation from classical cratering onto a solid substrate, it is sufficient for this analysis simply to determine whether small (km-scale) impactors are able to penetrate the thick lunar crust.

The penetration depth of an impactor is estimated using crater-projectile scaling laws, with the assumption that HSEs are delivered to the mantle only when the depth of the impact crater exceeds the typical crustal thickness. We use the scaling law from Allibert et al. (2023) for the maximum crater depth (Z_{crater}), which captures the transition between sub- and supersonic impacts by separating the effects of the Mach number ($M = v_{\mathrm{imp}}/U_s$), and the Froude number ($Fr = v_{\mathrm{imp}}^2/gR_{\mathrm{imp}}$),

$$\frac{Z_{\mathrm{crater}}}{R_{\mathrm{imp}}Fr^{1/4}} = a\left(1 + bM^2\right)^{-c}. \tag{17}$$

Here R_{imp} is the impactor radius, g the acceleration due to gravity of the Moon, and $(a, b, c) = (1.092, 0.11, 0.25)$ best-fit parameters. We assume a value for the sound speed of $U_s = 4472\,\mathrm{ms}^{-1}$ (Allibert et al., 2023). The impact velocity is calculated following Lissauer et al. (1988) as

$$v_{\mathrm{imp}}^2 = v_{\mathrm{esc,L}}^2 + v_{\mathrm{rel}}^2 + 3v_{\mathrm{kep,L}}^2, \tag{18}$$

where $v_{\mathrm{kep,L}}$, $v_{\mathrm{esc,L}}$ are the orbital, and escape velocity of the Moon respectively, and v_{rel} is the impactor's relative velocity (allowing for easy comparison with the characteristic velocity dispersion of a collisionally damped disk; Schlichting et al., 2012). Considering the maximum crater depth ensures our results are conservative: while several post-impact processes, such as jet formation during crater collapse, will limit the penetration depth of an impactor (e.g., Landeau et al., 2021; Allibert et al., 2023; Engels et al., 2024), no HSEs will reach the lunar mantle if the maximum crater depth is less than the crustal thickness.

Maximum crater depth, as a function of impact velocity, is shown in figure 6, demonstrating that small ($\lesssim 1\,\mathrm{km}$) impactors are unable to deliver any appreciable concentration of HSEs to the lunar mantle – in agreement with detailed hydrocode simulations of lunar impacts (Jackson et al., 2023). These impactors will predominantly (if not uniquely) deliver HSEs to the lunar crust, which is in clear disagreement with observational constraints (e.g., Ryder, 2002; Day & Walker, 2015). While it is not clear exactly when the modern lunar crust was established, we note that models support the rapid formation of a thick flotation crust as the lunar magma ocean cools (Elkins-Tanton et al., 2011). Any HSEs delivered by impactors penetrating a shallow early crust would be subsequently stripped from the mantle, and would therefore not contribute to observed HSEs (e.g., Rubie et al., 2016; Morbidelli et al., 2018). It is therefore impossible to simultaneously match both the observed Earth-Moon HSE ratio, and the concentration of HSEs in the lunar mantle via the delivery of small impactors.

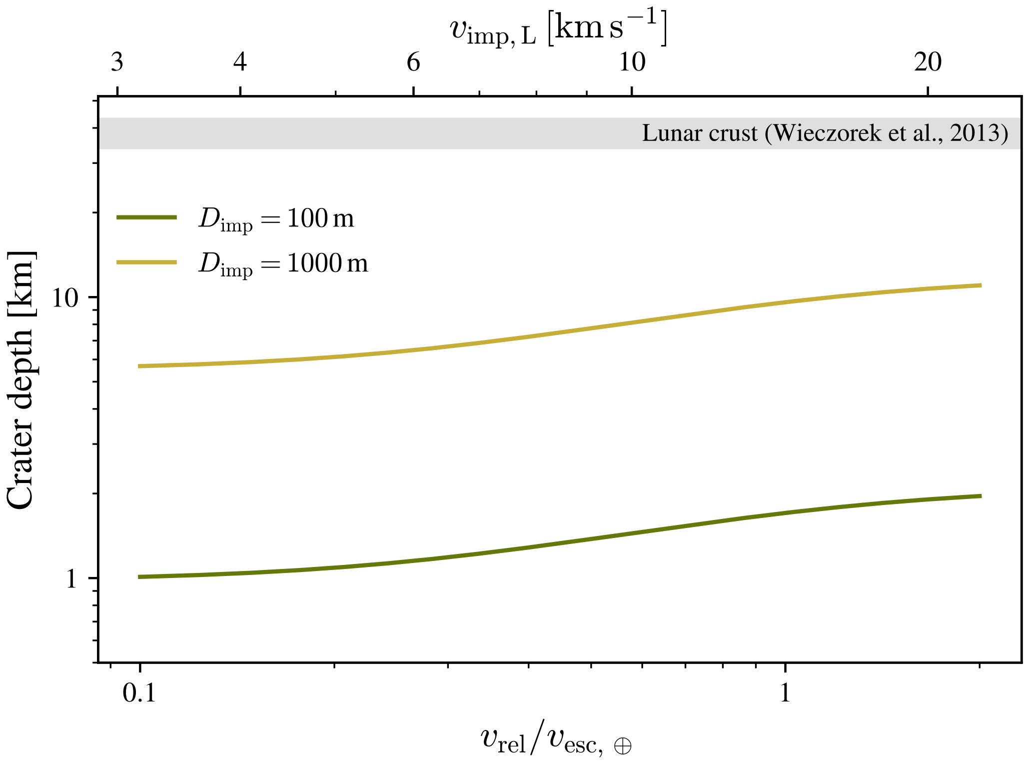

Figure 6. The impact crater depth, Z_{crater}, is calculated as a function of relative velocity, v_{rel}, for 100 and 1000 m diameter impactors. Corresponding impact velocities, $v_{\mathrm{imp,L}}$, on the surface of the Moon (calculated using equation 18) are included for reference. We use the Allibert et al. (2023) scaling law when calculating the crater depth. In all cases, the impactors are unable to penetrate the lunar crust, which has an average depth of roughly 34 - 43 km (Wieczorek et al., 2013).

3.3 Summary: the delivery of HSEs by small impactors

We have shown in this section that for all observed HSEs to be delivered by small ($\lesssim 1$ km) impactors during the late veneer, an unrealistically large mass ($\lesssim M_{\oplus}$) would also be delivered by larger bodies, the metallic fraction of which lost to Earth's core. Thus, the only way to avoid such a mass-accretion catastrophe would be if there was a dearth of large impactors during the late veneer (i.e., a population of only sub-km impactors). We demonstrated this would also be incompatible with observational constraints, delivering HSEs predominantly (perhaps uniquely) to the lunar crust, rather than mantle. The delivery of HSEs via the direct, convective entrainment of small planetesimals is therefore unable to account for observed mantle HSEs.

4 Summary and Discussion

In §2 we demonstrated that impactors larger than ~ 1 km will typically penetrate Earth's crust, and generate significant silicate melt from both the target and impactor. Using analytical scaling relations, we showed that metals from these impactors will collect at the bottom of melt pools, and that subsequent diapirism will result in HSE loss to Earth's core. However, in order to deliver sufficient mass in small impactors to account for Earth's HSEs, we demonstrated in §3 that an implausibly large mass ($\lesssim M_{\oplus}$) would also be delivered by larger bodies in a collisional size distribution. Metals from these impactors will quickly sink to Earth's core, leaving no HSE signature in the mantle.

To avoid such a mass accretion catastrophe, our results therefore suggest that large impactors must make a significant contribution to observed mantle HSE abundances. In §4.1 we identify two potential resolutions to this apparent paradox, which circumvent the challenges associated with the entrainment of metal diapirs described in §2. There must either exist some mechanism(s) through which HSEs, sequestered in the metallic cores of large differentiated impactors, contribute to mantle HSEs, or there was alternatively the delivery of a significant quantity of oxidised (carbonaceous chondrite-like) material during the late veneer.

In either case, there remains significant uncertainty in the efficiency of HSE delivery, and therefore total mass accretion during the late veneer. Assuming the delivery of HSEs with efficiency f (whether due to the physical mechanism(s) of HSE delivery from differentiated impactors, or the mass fraction of oxidised material delivered to Earth) total mass accretion during the late veneer will be a factor $1/f$ times larger than traditional estimates. An efficiency less than 10% would imply the late accretion of $\gtrsim 5\,\mathrm{wt\%}$ of Earth's mass. We discuss in §4.2 the viability of such a large increase in total mass accretion in the context of four independent constraints, and comment in §4.3 on the main assumptions we have made that could affect our conclusions.

4.1 Two potential resolutions to the mass accretion catastrophe

4.1.1 HSE delivery from the cores of large, differentiated impactors

One possibility is that large, differentiated impactors successfully contribute to observed mantle HSEs. This would require the disruption of impactor core material into $\lesssim 0.01\,\mathrm{mm}$ fragments, so that its metals can be convectively entrained in the impact-generated magma pond (see §2.2). We reiterate, however, that this required fragment size is at least one order of magnitude smaller than is expected after an impact (Deguen et al., 2014; Maller et al., 2024), and there is presently little consensus regarding the physical mechanism(s), and efficiency of HSE delivery from the cores of differentiated planetesimals. Estimates of total mass accretion during the late veneer are therefore, currently, unconstrained.

Previous studies have focused on the accretion of lunar-sized impactors, highlighting that mass accretion may occur over a prolonged period of time due to non-merging collisions (Genda et al., 2017), or invoking the presence of a partially molten zone beneath impact-generated magma oceans (Korenaga & Marchi, 2023). The efficiency of HSE delivery from the unavoidable collisions of smaller bodies (figure 1) remains, however, unclear. The cumulative contribution from these smaller bodies to Earth's mantle HSEs is therefore (currently) unconstrained and could, depending on the leftover planetesimal's SFD, significantly bias estimates of total mass accretion (see § 3.1). Moreover, we note that recent dynamical simulations record very few impacts of lunar-sized embryos onto the terrestrial planets post-Moon formation (e.g., Woo et al., 2024).

It is possible instead that the accretion of a lunar-sized embryo is not required to account for observed HSEs. Promisingly, several recent studies (Kraus et al., 2015; Li et al., 2020; Saurety et al., 2025) suggest that vapor production during large impacts has been largely underestimated during late accretion, which following the condensation and rain-out of vaporised core material, could distribute small metal droplets globally across Earth's surface. While our results (see §2) demonstrate that non-vaporised metals will sink to Earth's core, the global transport of vaporised impactor core material may in principle be able to account for a significant proportion of observed HSEs (Albarède et al., 2013; Kraus et al., 2015). It is possible also that the relative dearth of lunar HSEs may arise naturally in this scenario, given the large characteristic expansion velocity of vaporised core material and low lunar escape velocity (Kraus et al., 2015).

The global distribution of Ir-rich metal nuggets in the clay layer at the K-Pg boundary is thought to be consistent with condensation from the vaporised ejecta of the ($D \sim 10\,\mathrm{km}$) Chicxulub impactor (Goderis et al., 2021), and provides some tentative observational evidence in support of the efficient delivery of HSEs via vaporisation. We note, however, that the typical size of metal droplets condensed from a vapor cloud (of crucial importance for their subsequent entrainment in a turbulent magma ocean, see § 2.2) depends sensitively on both impactor diameter and impact velocity (Johnson & Melosh, 2012). For large planetesimals (i.e., $D \gtrsim 100\,\mathrm{km}$), the average spherule diameter is 2–3 orders of magnitude larger than the critical droplet size $d \approx 0.01\,\mathrm{mm}$ (see figure 13, Johnson and Melosh (2012)). We therefore expect that only spherules advected away from newly-formed magma ponds will effectively contribute to observed HSEs.

The vaporisation of core material therefore presents a promising avenue through which HSEs may be delivered via large, differentiated planetesimals, which will be explored in detail in future work.

4.1.2 HSE delivery from carbonaceous chondrite-like impactors

Alternatively, the delivery of significant quantities of oxidised carbonaceous chondrite-like material (i.e., arriving with no metal phase) would prevent the efficient loss of metals to Earth's core – given there will be no excess density relative to the silicate melt – and thereby help avoid a mass accretion catastrophe. The chemical composition of the late veneer is, however, a matter of longstanding debate (e.g., Marty, 2012; Fischer-Gödde & Kleine, 2017). Recently however, Ruthenium isotope measurements have been argued to support the late delivery accretion of a large mass fraction ($\sim 60\%$) of CM chondrite-like material (Fischer-Gödde et al., 2020). Burkhardt et al. (2021) report a slightly lower fraction ($\sim 30\%$) on the basis of the bulk silicate Earth's Mo, supporting a substantive carbonaceous contribution to Earth's late accretion.

This picture is supported by recent studies demonstrating that the accretion of undifferentiated CC-like bodies could account for a significant fraction of Earth's Zn budget (Martins et al., 2023, 2024). We note further that, no matter the timing of the Moon-forming impact, the late accretion of approximately 30% carbonaceous chondrites is recovered by dynamical simulations of solar system formation in the context of an early instability (Joiret et al., 2024), in agreement with these recent geochemical constraints.

Given that HSEs from the remaining fraction of reduced impactors will still be lost to Earth's core, estimates of total mass accretion remain accordingly very sensitive to the mass fraction of oxidised impactors delivered during the late veneer (see figure 7). The late accretion of 30 % carbonaceous chondrite-like material during the late veneer, as reported in Burkhardt et al. (2021), would require total mass accretion only ~ 3 times larger than traditional estimates, which is likely consistent with independent constraints on total mass accretion to the early Earth (see §4.2). We note, however, that while able to account for the delivery of HSEs to Earth's mantle, it remains challenging to explain the high Earth-Moon HSE ratio in this scenario, particularly given that the stochastic accretion of lunar-sized embryos post-Moon formation is not commonly observed in dynamical simulations of terrestrial planet formation (e.g., Woo et al., 2024).

4.2 How much excess mass accretion can the Earth-Moon system accommodate?

First, increased mass accretion during the late veneer would have significant implications for the geological evolution of the Hadean Earth, causing the mixing, burial,

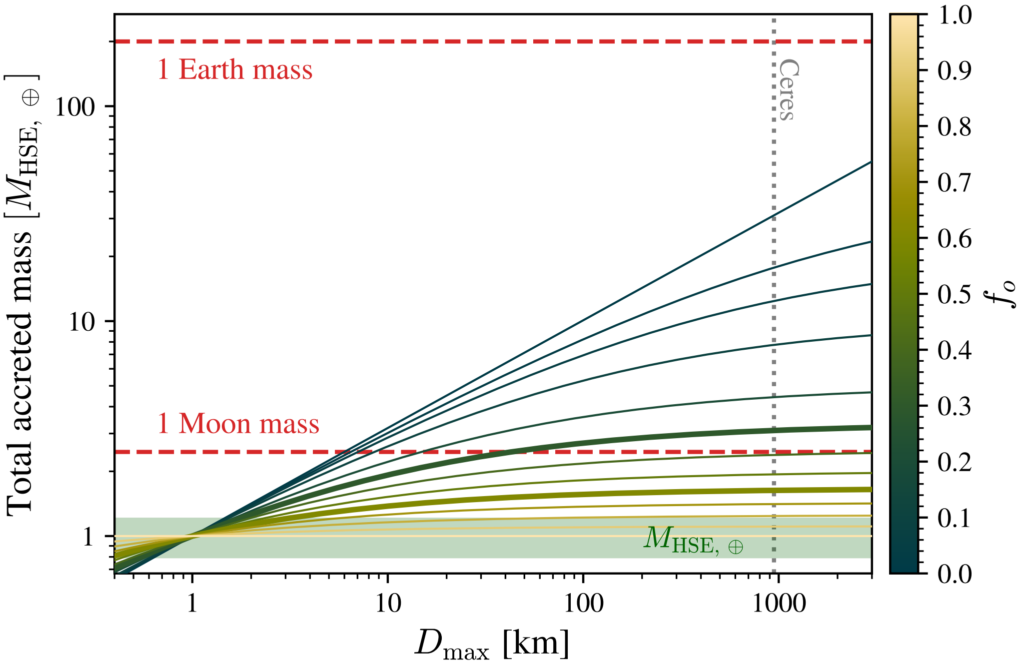

Figure 7. Total mass accretion to the Earth is calculated as a function of maximum impactor diameter, D_{max}, assuming a collisional size distribution ($n(D)dD \propto D^{-7/2}dD$; Dohnanyi, 1969). All impactors smaller than $D_{\mathrm{crit}} = 1\,\mathrm{km}$ are assumed to be entrained in Earth's mantle. Moreover, a mass fraction f_o of larger planetesimals are assumed to have no metal phase, and therefore also contribute to mantle HSE signatures. This calculation, following closely the analysis in §3.1, is described in detail in Appendix C. The bold green line corresponds to $f_o = 0.6$, the mass fraction reported in Fischer-Gödde et al. (2020); the bold blue line corresponds to $f_o = 0.3$, as reported in Burkhardt et al. (2021). Total mass accretion will increase for steeper SFDs (as inferred for the main asteroid belt, and expected for the streaming instability; see figure 5), therefore requiring a more oxidised late veneer in order to avoid a mass accretion catastrophe.

and melting of its early crust. The cumulative delivery of $\sim 0.15\,\mathrm{wt}\%$ over 100 Myr is able to (subject to assumptions about crustal thickness) melt all of Earth's crust (Mojzsis et al., 2019), whilst Marchi et al. (2014) claim this bombardment would comfortably bury Earth's crust under impact melt. Mass fluxes in excess of $\sim 5\,\mathrm{wt}\%$ would therefore be strongly in tension with the existence of zircons dating to 4.4 Gya (Valley et al., 2014), which would not survive such an intense period of late accretion.

Second, there exist additional isotopic constraints on late accretion thanks to the isotopic similarity of the Earth, and Moon. These include the difference in ^{182}W between the Earth and Moon, which has been attributed to the late accretion of $\sim 0.7\,\mathrm{wt}\,\%$ of chondritic material (Touboul et al., 2015; Kruijer et al., 2015). Jacobson et al. (2014) also infer an upper limit for late accretion of about $0.01\,M_\oplus$, based on the O and Ti isotopic similarity of the Earth and Moon. Given the approximate consensus between these separate isotopic constraints, it appears likely that mass accretion significantly in excess of $0.01\,M_\oplus$ would require increasingly fine-tuned assumptions about the isotopic compositions of late accreted planetesimals.

Third, various dynamical simulations find a negative correlation between the late veneer mass, and the timing of the Moon-forming impact (e.g., Jacobson et al., 2014; Woo et al., 2024). This has a simple qualitative explanation; there will be fewer available planetesimals to source a late veneer at later times (a consequence of collisions with planets, ejection onto hyperbolic orbits, and catastrophic collisions with other planetesimals). Whilst these results are clearly model-specific, both Jacobson et al. (2014) and Woo et al. (2024) suggest the late accretion of $\sim 5\,\mathrm{wt}\%$ would require Moon-formation earlier than $\sim 20\,\mathrm{Myr}$ after the condensation of the first solids in the solar system. This is highly inconsistent with the date of the Moon forming impact, as recorded by various radioactive chronometers (e.g., Kleine et al., 2005; Touboul et al., 2007).

Fourth, impact-generated satellites (e.g, the Moon) are very sensitive to ongoing accretion (Pahlevan & Morbidelli, 2015). Impacts onto the Earth are typically preceded by many ($\sim 10^4$) collisionless encounters, which efficiently transfer angular momentum to the Moon. The late accretion of $\sim 5\,\mathrm{wt}\%$ would therefore likely drive significantly increased orbital excitation of the Moon, and most likely its dynamical loss (Pahlevan & Morbidelli, 2015). We note, requiring earlier Moon-formation to accommodate the late delivery of $\sim 5\,\mathrm{wt}\%$ seems particularly incompatible with the long-term stability of the Moon's orbit.

It is therefore highly improbable that the late delivery of HSEs to Earth's mantle was particularly inefficient (i.e., less than $\sim 10\%$), given this would imply a large mass flux inconsistent with several independent constraints on total mass accretion to the Hadean Earth.

4.3 Model limitations

There are a number of caveats to our conclusions, concerning both the entrainment of metals in the mantle, and the implications for Earth's accretion history. We summarise the most important here.

Estimates of excess mass accretion during the late veneer, leaving no mantle HSE signature, are sensitive to the critical impactor diameter, D_{crit}. As motivated in §2.1, D_{crit} roughly separates the efficient and inefficient delivery of HSEs to Earth's mantle (from smaller and larger bodies respectively). We identify criteria for melting, and penetrating Earth's crust as crucial in determining D_{crit}. Our analysis does not, however, account for all relevant physical processes, and it is therefore possible that we over-, or underestimate the true value of D_{crit}. This uncertainty will accordingly decrease (increase) excess mass accretion during the late veneer. As shown in Figure 5, however, an order of magnitude increase in D_{crit} would still imply total mass accretion incompatible with several independent constraints (§4.2). Unless this critical diameter is much larger than $\sim 10\,\mathrm{km}$, this uncertainty is unlikely to alter our main conclusion: small planetesimals are unable to account for observed HSEs, and there is correspondingly significant uncertainty in total mass accretion during the late veneer.

The entrainment of metals in a magma pond is very sensitive to the radius of the metal drops, an empirically determined efficiency factor (ϵ), and the heat flux at the surface of the magma pond (F). The radius of metal drops following a planetary impact is however poorly known, and estimates for this empirical efficiency factor ϵ differ by nearly a factor of 5 (V. S. Solomatov et al., 1993; Lavorel & Le Bars, 2009). Accordingly, there is uncertainty in the equilibrium mass of suspended metal, as is evident in figure 3. Even when taking end-member values for each parameter (ϵ and F), it is not possible to account for Earth's HSEs. For our conclusions to change significantly, alternative fragmentation mechanisms must exist that can generate metal drops smaller than 0.01 mm. We reiterate, however, that currently this remains at least one order of magnitude below best-estimates (Deguen et al., 2014; Maller et al., 2024), and any mechanism capable of achieving this remains elusive.

As discussed in §2.2, the condition used to determine the entrainment of metal drops in a magma pond ($\theta_S > \theta_c$) has only been demonstrated for solid particles (V. S. Solomatov et al., 1993; Sturtz et al., 2021). This has not however been tested for liquid drops, and there is therefore uncertainty in our results regarding the critical drop size for entrainment. Liquid drops can in principle merge with the bottom layer, and it is therefore possible that surface tension may in fact decrease the efficiency of this re-entrainment processes. We therefore expect that our conclusions still hold despite the lack of experiment on the sedimentation of dilute liquid drops in magma oceans.

Finally, the condition used to determine the entrainment of metal diapirs in a solid, or partially solid, mantle neglects the possible deformation of the diapir by the convective flow and the multiphase dynamics of mushy, solidifying magma oceans (Ballmer et al., 2017; Maurice et al., 2017; Morison et al., 2019; Labrosse et al., 2024; Boukaré et al., 2025). Quantifying these effects requires further investigation using numerical simulations of convecting mushy magma oceans, which is beyond the scope of this paper.

5 Conclusions

As recorded by the elevated concentrations of HSEs in the mantle, the late veneer is thought to deliver at least $\sim 0.5\,\mathrm{wt\%}$ (of Earth's mass) of chondritic material to the Earth, and $\sim 0.02\,\mathrm{wt\%}$ to the Moon (Day et al., 2016). A consequence of the negative buoyancy of metals in both fully liquid magma ponds and the solid mantle, however, is that the entrainment of HSEs in Earth's mantle is much more challenging than previously thought. We demonstrate in this study that there exists a critical diameter ($\sim 1\,\mathrm{km}$), separating the efficient and inefficient delivery of HSEs to the mantle, with the direct entrainment of HSEs possible only for smaller impactors via the tectonic recycling of the crust. However, despite the potentially efficient delivery of metals to Earth's mantle by small impactors, we demonstrate that they cannot be the dominant source of Earth's HSEs. In order to deliver sufficient mass in sub-km bodies, we show there would be an implausibly large mass ($\lesssim 1\,M_\oplus$) delivered by larger ($D > 1\,\mathrm{km}$) bodies in a collisional size distribution, with their HSEs lost to Earth's core. There is therefore, currently, a contradiction between the observed concentrations of HSEs in the mantle, the geodynamics of metal entrainment, and estimates of total mass accretion during the late veneer.

To avoid such a mass accretion catastrophe, we suggest impactors larger than $1\,\mathrm{km}$ must make significant contributions to mantle HSE signatures, and identify two potential resolutions to this apparent paradox. We show that it would be possible to suspend sufficient HSEs in an impact-generated magma pond, if there exists mechanisms able to disrupt impactor core material into $\lesssim 0.01\,\mathrm{mm}$ fragments during large planetary impacts. This is, however, at least one order of magnitude smaller than current estimates for the size of metal drops after impacts. Alternatively, the delivery of a significant mass fraction of oxidised material during the late veneer would prevent the loss of metals to Earth's core, thereby avoiding such a mass accretion catastrophe. In both scenarios, total mass accretion during the late veneer remains unconstrained, due to uncertainty in the efficiency of physical mechanisms capable of disrupting impactor core material into sufficiently small fragments, and the mass fraction of oxidised material delivered to Earth during the late veneer.

Appendix A The condition for melting by impact

A1 Quantification of impact-induced melting

The fate of impactor material is dependent on the peak pressure experienced during the compression stage of crater formation, as this will directly determine the density, and temperature of impactor material. Regions of impactor material will melt (va-

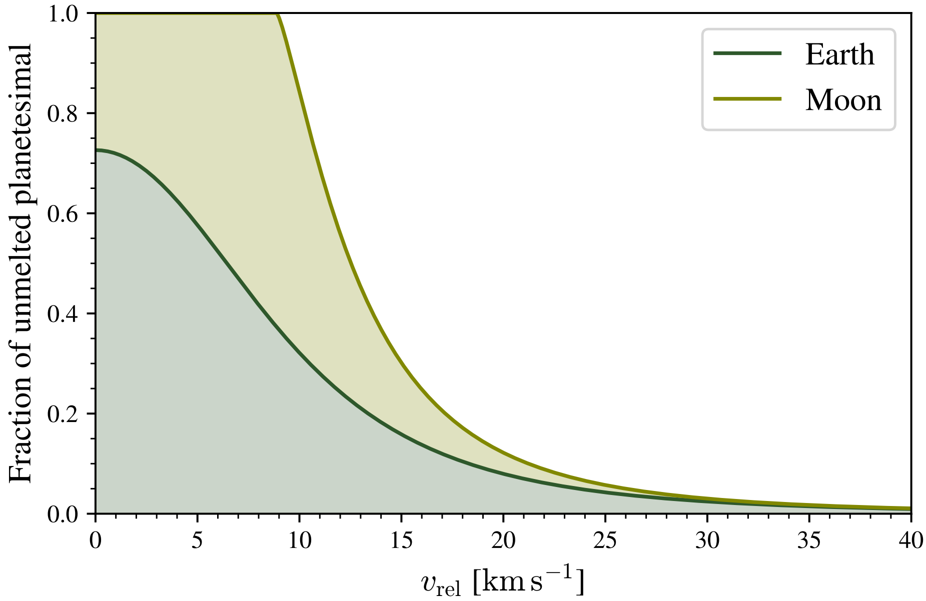

Figure A1. The fraction of unmelted impactor material is plotted as a function of relative velocity, $v_{\rm rel}$, for both the Earth and Moon. This is calculated using the parameterisation for asteroid survivability from Potter and Collins (2013), assuming a critical shock pressure for melting of 106 GPa (Wünnemann et al., 2008). The material constants $(C_i, S_i) = (5.430\,\mathrm{km\,s^{-1}}, 1.34)$ and $(C_t, S_t) = (3.816\,\mathrm{km\,s^{-1}}, 1.28)$ are chosen for a dunite impactor and granite target (Table 1; Potter & Collins, 2013). Significant melting will occur onto both the Earth and Moon for a typical relative velocity of 15 km s^{-1}.

porise) if they experiences peak shock pressures in excess of the material's incipient melting (vaporisation) shock pressure.

The distribution of shock pressure within projectiles is however highly complex, and so detailed hydrocode simulations are necessary to accurately determine the fate of impactor material (e.g., Pierazzo & Melosh, 2000; Potter & Collins, 2013). Here, we use the results from iSALE simulations in Potter and Collins (2013) to estimate the fraction of impactor material that does not melt,

$$f = 1 - \cos^{1.3}\left(\frac{\pi}{2}\frac{P_{\rm melt}}{P_{\rm max}\sin\theta}\right), \tag{A1}$$

where $P_{\rm melt}$ is the critical shock pressure for incipient melting (assumed to be the ANEOS-derived value of 106 GPa for dunite projectiles; Wünnemann et al., 2008), $P_{\rm max}$ the peak shock pressure experienced anywhere in the impactor, and θ the impact angle. Note, the choice of dunite as a proxy for asteroidal composition ensures that our estimated critical impactor size for melting, $D_{\rm crit}$ provides an upper limit, given the critical pressure for melting is significantly lower for other rock types (Wünnemann et al., 2008).

The peak shock pressure, $P_{\rm max}$, is estimated using the planar shock approximation, which is relatively accurate for materials with a linear shock-particle velocity relationship (i.e., $U = C + Su$, where C and S are empirically determined parameters describing target, or impactor material; Melosh, 1989). The peak pressure is given by the Hugoniot equation

$$P_{\rm max} = \rho_{0i} u_i \left(C_i + S_i u_i\right), \tag{A2}$$

where ρ_{0i} is the uncompressed impactor density, and u_i the impactor particle velocity. This peak pressure increases with impact velocity, $v_{\rm imp}$, through its dependence on the particle velocity, which is given by

$$u_i = \frac{-B + \sqrt{B^2 - 4AC}}{2A}, \tag{A3}$$

where

$$A = \rho_{0i} S_i - \rho_{0t} S_t, \tag{A4}$$
$$B = \rho_{0i} C_i + \rho_{0t} C_t + 2\rho_{0t} S_t v_{\rm imp}, \tag{A5}$$
$$C = -\rho_{0t} v_{\rm imp} \left(C_t + S_t v_{\rm imp} \right), \tag{A6}$$

with the subscripts i, t referring to impactor and target material respectively.

The fraction of unmelted impactor material is plotted as a function of relative velocity, $v_{\rm rel}$, in Figure A1. The corresponding impact velocities on the Moon and Earth are given by

$$v^2_{\rm imp,\oplus} = v^2_{\rm esc,\oplus} + v^2_{\rm rel}, \tag{A7}$$
$$v^2_{\rm imp,L} = v^2_{\rm esc,L} + 3v^2_{\rm kep,L} + v^2_{\rm rel} \tag{A8}$$

respectively (e.g., Lissauer et al., 1988), allowing for easy comparison between impacts on the Earth and Moon.

A2 The atmospheric entry of planetesimals

Impactors entering Earth's atmosphere are subject to large ram pressures, often leading to the significant deceleration and fragmentation of small bodies. The size and velocity of impactors arriving at the top of Earth's atmosphere may therefore be considerably different to those reaching the surface. Here we determine the minimum impactor diameter for melting, assuming a critical impact velocity of $15\,\mathrm{km\,s^{-1}}$ (as determined in the previous section).

The trajectory of an impactor through the atmosphere is first described by a set of four coupled differential equations (e.g., Passey & Melosh, 1980), before fragmentation occurs when the ram pressure exceeds the bodies tensile strength. Detailed modelling of fragmentation is however challenging, given the complex physical processes involved. We thus use the simple 1D model from Chyba et al. (1993), which is able to reproduce the observed energy deposition of Tunguska-like impactors, describing the deformation (or "pancaking") of impactor material into a cylindrical shape.

We assume the impactor will fragment into a number of small pieces (in an airburst-like event) when the radius of the impactor reaches 6 times its initial value (following Chyba et al., 1993). To determine the critical diameter for melting, we numerically calculate the trajectory of a stony projectile, varying its initial diameter until it is able to reach the surface intact, with velocity greater than $15\,\mathrm{km\,s^{-1}}$. We assume an isothermal atmospheric profile, with a scale height of 7 km, and vary the atmospheric surface density.

The results of this calculation are shown in figure A2, in which we see for a 1 bar atmosphere, the critical radius for melting, R_m, is roughly 50 m. This increases to roughly 1000 m for a 100 bar atmosphere, reflecting the increased ram pressure experienced by the impactor.

Appendix B Metal drop size distribution in impact-generated magma pond

Recent results on the size distribution of bubbles in a turbulent flow (e.g., Rivière et al., 2022) demonstrate that the drop size distribution follows a power law. Below the

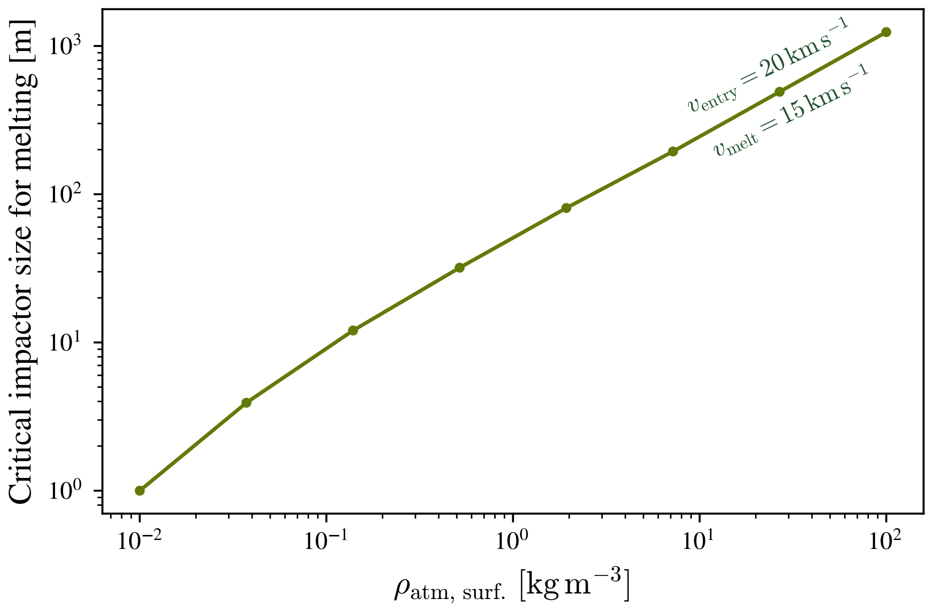

Figure A2. The critical impactor size for melting is calculated as a function of atmospheric surface density, $\rho_{\text{atm,surf.}}$, using the deformation model from Chyba et al. (1993), assuming an isothermal atmospheric profile with a constant scale height of 8 km. A constant entry velocity of $20\,\mathrm{km\,s^{-1}}$ is used, with significant melting expected for impact velocities in excess of $15\,\mathrm{km\,s^{-1}}$ (see figure A1).

Hinze scale, at which surface tension equilibrates local pressure fluctuations – expected to determine the mean drop size in an impact-generated magma ocean (Deguen et al., 2014; Wacheul & Le Bars, 2018) – drop size scales as $n(d) \propto d^{-3/2}$, where d is the drop diameter (Rivière et al., 2022). For such a power law, the mass in drops of size d varies as $m(d) \propto d^{3/2}$, meaning that the total metal mass is dominated by the largest drops present in the magma ocean. Here we demonstrate that, while small drops of size ~ 0.01 mm might be present in a magma ocean, they will carry insufficient mass to account for Earth's HSEs.

We consider a distribution of metal drops with diameters in the range $[d_{\text{min}}, d_{\text{max}}]$, where $d_{\text{max}} \gg d_{\text{min}}$ is the size of the largest drops in the impact-generated magma. Figure 3 demonstrates that only metal drops smaller than $d_{\text{ent.}} \sim 0.01$ mm can potentially be entrained with sufficiently high volume ratio to explain Earth's HSEs. The total mass in suspended drops ($d \leq d_{\text{ent.}}$) is thus given by

$$\frac{M(d \leq d_{\text{ent.}})}{M_{\text{HSE},\oplus}} = \frac{d_{\text{ent.}}^{5/2} - d_{\text{min}}^{5/2}}{d_{\text{max}}^{5/2} - d_{\text{min}}^{5/2}} \sim \left(\frac{d_{\text{ent.}}}{d_{\text{max}}}\right)^{5/2}. \tag{B1}$$

From equation B1 it is clear that the required late veneer mass must significantly exceed $M_{\text{HSE},\oplus}$ when $d_{\text{ent.}} < d_{\text{max}}$. This is illustrated in figure B1, which shows the required late veneer mass as a function of d_{max}, assuming that HSEs were delivered by metal drops smaller than $d_{\text{ent.}} = 0.01$ mm, 0.03 mm, and 0.1 mm. Assuming the largest drops have a diameter ~ 1 mm (Deguen et al., 2014; Wacheul & Le Bars, 2018; Maller et al., 2024), this would require an implausibly large late accreted mass of $300 M_{\text{HSE},\oplus} \sim M_{\oplus}$. Thus, while there will be a distribution of droplets produced following a large impact, extending down to small sizes, these small drops will collectively carry insufficient mass to account for Earth's HSEs.

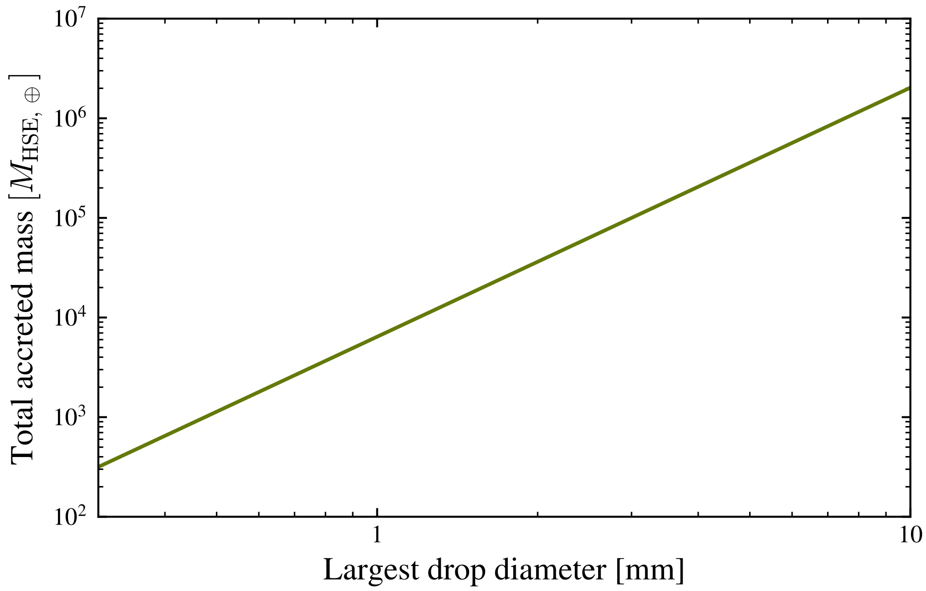

Figure B1. The required late veneer mass is calculated as a function of the largest drop diameter, assuming that HSEs were delivered in drops of diameter smaller than 0.03 mm, which could be entrained in significant proportions in the impact-generated magma. The drop size distribution is assumed to follow a $d^{-3/2}$ power-law, where d is the drops diameter (Rivière et al., 2022). With the largest drop size expected to be $\sim$ 1 mm (Deguen et al., 2014; Wacheul & Le Bars, 2018; Maller et al., 2024), this would require an unreasonably late accreted mass in excess of 300 $M_{\mathrm{HSE},\oplus}$.

Appendix C An oxidized late veneer

The accretion of oxidised carbonaceous-chondrite material during the late veneer is one potential way to avoid the loss of metal, and its HSEs, to Earth's core (as described in §2). This material, arriving with no (or very small amounts) metal phase present will efficiently contribute its HSEs to the mantle, by virtue of its much smaller density contrast with the surrounding silicates.

Here, we present a simple calculation assuming some constant (i.e., size-independent) fraction f_o of material arrives with no metal phase, with its HSEs accordingly distributed throughout its silicate components, and therefore contributes to observed HSE signatures. Following our approach in §3.1, we assume a collisional size distribution ($n(D)dD = KD^{-7/2}dD$ Dohnanyi, 1969), and assume all impactors smaller than $D_{\mathrm{crit}} = 1$ km are also entrained in Earth's mantle. The SFDs constant of proportionality, K, is now given by

$$K = \left(\frac{6M_{\mathrm{HSE},\oplus}}{\pi\rho_{\mathrm{imp}}}\right)\left[\int_{D_{\mathrm{min}}}^{D_{\mathrm{crit}}} D^{3-\alpha}dD + f_o\int_{D_{\mathrm{crit}}}^{D_{\mathrm{max}}} D^{3-\alpha}dD\right]^{-1}. \tag{C1}$$

Total mass accretion is therefore

$$M_{\mathrm{acc,tot}} = M_{\mathrm{HSE},\oplus}\left[\frac{\int_{D_{\mathrm{min}}}^{D_{\mathrm{max}}} D^{3-\alpha}dD}{\int_{D_{\mathrm{min}}}^{D_{\mathrm{crit}}} D^{3-\alpha}dD + f_o\int_{D_{\mathrm{crit}}}^{D_{\mathrm{max}}} D^{3-\alpha}dD}\right], \tag{C2}$$

which reverts exactly to equation 16 in the limit $f_o \to 0$, as expected. Total mass accretion, as a function of the SFDs maximum impactor diameter D_{max}, is shown in Figure 7. Increasing the mass fraction of oxidised material delivered (i.e., increasing f_o) effectively helps avoid the mass accretion catastrophe. Total mass accretion will remain less than 1 Moon mass provided $f_o \gtrsim 0.4$, which is smaller than the mass fraction reported in Fischer-Gödde et al. (2020). This is only ~ 3 times larger than traditional estimates of total mass accretion during the late veneer, and is likely consistent with independent constraints on total mass accretion to the Hadean Earth (see §4.2).

It is a significant simplification to assume the oxidation state of planetesimals is size-independent, and it is possible instead that this fraction could decrease significantly for larger bodies able to form a metallic core. This would significantly increase total mass accretion, and we would quickly return to the mass accretion catastrophe described in §3, given that total mass is concentrated within the largest bodies in a collisional size distribution.

Evidence from within the Solar System is, however, not totally conclusive. Whilst some oxidised bodies formed with metallic, iron-rich cores, as is evidenced by both iron meteorites (Grewal et al., 2024) and the water-rich Jovian satellite Ganymede (Schubert et al., 1996), Ceres (the largest body in the asteroid belt) demonstrates that others did not (Thomas et al., 2005). We therefore, in the interests of simplicity, assume this fraction is size-independent, and note this has the potential to significantly bias the results shown in figure 7.

Open Research Section

No new data were generated for this work. Scripts used to generate the figures presented in this work are publicly available at `https://github.com/richard17a/HSE_mass_accretion`. This repository will be archived in Zenodo upon acceptance.

Acknowledgments

We thank Helen Williams, Ingrid Blanchard, and Julien Siebert for useful discussions. R.J.A. acknowledges the Science and Technology Facilities Council (STFC) for a PhD studentship. A.B. acknowledges the support of a Royal Society University Research Fellowship, URF/R1/211421. This work was supported by the Programme National de Planétologie (PNP) of CNRS-INSU, co-funded by CNES.

References

Agrusta, R., Morison, A., Labrosse, S., Deguen, R., Alboussière, T., Tackley, P., & Dubuffet, F. (2020). Mantle convection interacting with magma oceans. *Geophysical Journal International*, *220*(3), 1878–1892.

Albarède, F., Ballhaus, C., Blichert-Toft, J., Lee, C.-T., Marty, B., Moynier, F., & Yin, Q.-Z. (2013, January). Asteroidal impacts and the origin of terrestrial and lunar volatiles. *Icarus*, *222*(1), 44-52. doi: 10.1016/j.icarus.2012.10.026

Allibert, L., Landeau, M., Röhlen, R., Maller, A., Nakajima, M., & Wünnemann, K. (2023, August). Planetary Impacts: Scaling of Crater Depth From Subsonic to Supersonic Conditions. *Journal of Geophysical Research (Planets)*, *128*(8), e2023JE007823. doi: 10.1029/2023JE007823

Andrault, D., Bolfan-Casanova, N., Nigro, G. L., Bouhifd, M. A., Garbarino, G., & Mezouar, M. (2011, April). Solidus and liquidus profiles of chondritic mantle: Implication for melting of the Earth across its history. *Earth and Planetary Science Letters*, *304*(1-2), 251-259. doi: 10.1016/j.epsl.2011.02.006

Ballmer, M. D., Lourenço, D. L., Hirose, K., Caracas, R., & Nomura, R. (2017). Reconciling magma-ocean crystallization models with the present-day structure of the earth's mantle. *Geochemistry, Geophysics, Geosystems*, *18*(7), 2785-2806. Retrieved from `https://agupubs.onlinelibrary.wiley.com/doi/abs/`

10.1002/2017GC006917 doi: https://doi.org/10.1002/2017GC006917

Blanchard, I., Siebert, J., Kubik, E., Minchenkova, A., Calvo, L., & Wehr, N. (2025). Earth's deep magma ocean never reached sulfide saturation. *Geochemical Perspectives Letters*, *34*, 6–10. Retrieved from https://www.geochemicalperspectivesletters.org/article2506 doi: https://doi.org/10.7185/geochemlet.2506

Blau, P. J., Axon, H. J., & Goldstein, J. I. (1973). Investigation of the canyon diablo metallic spheroids and their relationship to the breakup of the canyon diablo meteorite. *Journal of Geophysical Research*, *78*(2), 363–374.

Bottke, W. F., Durda, D. D., Nesvorný, D., Jedicke, R., Morbidelli, A., Vokrouhlický, D., & Levison, H. (2005, May). The fossilized size distribution of the main asteroid belt. *Icarus*, *175*(1), 111-140. doi: 10.1016/j.icarus.2004.10.026

Bottke, W. F., Walker, R. J., Day, J. M. D., Nesvorny, D., & Elkins-Tanton, L. (2010, December). Stochastic Late Accretion to Earth, the Moon, and Mars. *Science*, *330*(6010), 1527. doi: 10.1126/science.1196874

Boukaré, C.-É., Badro, J., & Samuel, H. (2025, April). Solidification of Earth's mantle led inevitably to a basal magma ocean. *Nature*, *640*(8057), 114-119. doi: 10.1038/s41586-025-08701-z

Boyet, M., & Carlson, R. W. (2005, July). ^{142}Nd Evidence for Early (¿4.53 Ga) Global Differentiation of the Silicate Earth. *Science*, *309*(5734), 576-581. doi: 10.1126/science.1113634

Brandon, A. D., Puchtel, I. S., Walker, R. J., Day, J. M. D., Irving, A. J., & Taylor, L. A. (2012, January). Evolution of the martian mantle inferred from the ^{187}Re- ^{187}Os isotope and highly siderophile element abundance systematics of shergottite meteorites. *Geochimica et Cosmochimica Acta*, *76*, 206-235. doi: 10.1016/j.gca.2011.09.047

Brandon, A. D., Walker, R. J., Morgan, J. W., & Goles, G. G. (2000, December). Re-Os isotopic evidence for early differentiation of the Martian mantle. *Geochimica et Cosmochimica Acta*, *64*(23), 4083-4095. doi: 10.1016/S0016-7037(00)00482-8

Brasser, R., Mojzsis, S. J., Werner, S. C., Matsumura, S., & Ida, S. (2016, December). Late veneer and late accretion to the terrestrial planets. *Earth and Planetary Science Letters*, *455*, 85-93. doi: 10.1016/j.epsl.2016.09.013

Brasser, R., Werner, S. C., & Mojzsis, S. J. (2020, March). Impact bombardment chronology of the terrestrial planets from 4.5 Ga to 3.5 Ga. *Icarus*, *338*, 113514. doi: 10.1016/j.icarus.2019.113514

Burkhardt, C., Spitzer, F., Morbidelli, A., Budde, G., Render, J. H., Kruijer, T. S., & Kleine, T. (2021, December). Terrestrial planet formation from lost inner solar system material. *Science Advances*, *7*(52), eabj7601. doi: 10.1126/sciadv.abj7601

Canup, R. M. (2008, August). Lunar-forming collisions with pre-impact rotation. *Icarus*, *196*(2), 518-538. doi: 10.1016/j.icarus.2008.03.011

Catling, D. C., & Zahnle, K. J. (2020, February). The Archean atmosphere. *Science Advances*, *6*(9), eaax1420. doi: 10.1126/sciadv.aax1420

Chopelas, A., & Boehler, R. (1992). Thermal expansivity in the lower mantle. *Geophysical Research Letters*, *19*(19), 1983–1986.

Chou, C. L. (1978, January). Fractionation of Siderophile Elements in the Earth's Upper Mantle. *Lunar and Planetary Science Conference Proceedings*, *1*, 219-230.

Chyba, C. F., Thomas, P. J., & Zahnle, K. J. (1993). The 1908 tunguska explosion: atmospheric disruption of a stony asteroid. *Nature*, *361*(6407), 40–44.

Citron, R. I., & Stewart, S. T. (2022, May). Large Impacts onto the Early Earth: Planetary Sterilization and Iron Delivery. *The Planetary Science Journal*, *3*(5), 116. doi: 10.3847/PSJ/ac66e8

Clesi, V., Monteux, J., Qaddah, B., Le Bars, M., Wacheul, J.-B., & Bouhifd, M.

(2020). Dynamics of core-mantle separation: Influence of viscosity contrast and metal/silicate partition coefficients on the chemical equilibrium. *Physics of the Earth and Planetary Interiors*, *306*, 106547. Retrieved from `https://www.sciencedirect.com/science/article/pii/S0031920119302456` doi: https://doi.org/10.1016/j.pepi.2020.106547

Costa, A. (2005). Viscosity of high crystal content melts: dependence on solid fraction. *Geophysical Research Letters*, *32*(22).

Dahl, T. W., & Stevenson, D. J. (2010, June). Turbulent mixing of metal and silicate during planet accretion — And interpretation of the Hf-W chronometer. *Earth and Planetary Science Letters*, *295*(1-2), 177-186. doi: 10.1016/j.epsl.2010.03.038

Dale, C. W., Burton, K. W., Greenwood, R. C., Gannoun, A., Wade, J., Wood, B. J., & Pearson, D. G. (2012, April). Late Accretion on the Earliest Planetesimals Revealed by the Highly Siderophile Elements. *Science*, *336*(6077), 72. doi: 10.1126/science.1214967

Day, J. M. D., Brandon, A. D., & Walker, R. J. (2016, January). Highly Siderophile Elements in Earth, Mars, the Moon, and Asteroids. *Reviews in Mineralogy and Geochemistry*, *81*(1), 161-238. doi: 10.2138/rmg.2016.81.04

Day, J. M. D., Paquet, M., & Timothy Jull, A. J. (2021a, April). Temporally limited late accretion after core formation in the Moon. *Meteoritics & Planetary Science*, *56*(4), 683-699. doi: 10.1111/maps.13646

Day, J. M. D., Paquet, M., & Timothy Jull, A. J. (2021b, April). Temporally limited late accretion after core formation in the Moon. *Meteoritics & Planetary Science*, *56*(4), 683-699. doi: 10.1111/maps.13646

Day, J. M. D., Pearson, D. G., & Taylor, L. A. (2007, January). Highly Siderophile Element Constraints on Accretion and Differentiation of the Earth-Moon System. *Science*, *315*(5809), 217. doi: 10.1126/science.1133355

Day, J. M. D., & Walker, R. J. (2015, August). Highly siderophile element depletion in the Moon. *Earth and Planetary Science Letters*, *423*, 114-124. doi: 10.1016/j.epsl.2015.05.001

de Koker, N. (2010, April). Thermal conductivity of MgO periclase at high pressure: Implications for the D̈region. *Earth and Planetary Science Letters*, *292*(3-4), 392-398. doi: 10.1016/j.epsl.2010.02.011

Deguen, R., Landeau, M., & Olson, P. (2014, April). Turbulent metal-silicate mixing, fragmentation, and equilibration in magma oceans. *Earth and Planetary Science Letters*, *391*, 274-287. doi: 10.1016/j.epsl.2014.02.007

Dohnanyi, J. S. (1969, May). Collisional Model of Asteroids and Their Debris. *Journal of Geophysical Research*, *74*, 2531-2554. doi: 10.1029/JB074i010p02531

Durda, D. D., Greenberg, R., & Jedicke, R. (1998, October). Collisional Models and Scaling Laws: A New Interpretation of the Shape of the Main-Belt Asteroid Size Distribution. *Icarus*, *135*(2), 431-440. doi: 10.1006/icar.1998.5960

Elkins-Tanton, L. T. (2008, July). Linked magma ocean solidification and atmospheric growth for Earth and Mars. *Earth and Planetary Science Letters*, *271*(1-4), 181-191. doi: 10.1016/j.epsl.2008.03.062

Elkins-Tanton, L. T., Burgess, S., & Yin, Q.-Z. (2011, April). The lunar magma ocean: Reconciling the solidification process with lunar petrology and geochronology. *Earth and Planetary Science Letters*, *304*(3-4), 326-336. doi: 10.1016/j.epsl.2011.02.004

Engels, T., Monteux, J., Boyet, M., & Bouhifd, M. A. (2024, August). Large impacts and their contribution to the water budget of the Early Moon. *Icarus*, *418*, 116124. doi: 10.1016/j.icarus.2024.116124

Fischer-Gödde, M., Elfers, B.-M., Münker, C., Szilas, K., Maier, W. D., Messling, N., ... Smithies, H. (2020, March). Ruthenium isotope vestige of Earth's pre-late-veneer mantle preserved in Archaean rocks. *Nature*, *579*(7798), 240-244. doi: 10.1038/s41586-020-2069-3

Fischer-Gödde, M., & Kleine, T. (2017, January). Ruthenium isotopic evidence for an inner Solar System origin of the late veneer. *Nature*, *541*(7638), 525-527. doi: 10.1038/nature21045

Fleck, J., Rains, C., Weeraratne, D., Nguyen, C., Brand, D., Klein, S., ... Olson, P. (2018). Iron diapirs entrain silicates to the core and initiate thermochemical plumes. *Nature communications*, *9*(1), 71.

Folco, L., Carone, L., D'Orazio, M., Cordier, C., Suttle, M. D., van Ginneken, M., & Masotta, M. (2022). Microscopic impactor debris at kamil crater (egypt): The origin of the fe-ni oxide spherules. *Geochimica et Cosmochimica Acta*, *335*, 297–322.

Freitas, D., Monteux, J., Andrault, D., Manthilake, G., Mathieu, A., Schiavi, F., & Cluzel, N. (2021, March). Thermal conductivities of solid and molten silicates: Implications for dynamos in mercury-like proto-planets. *Physics of the Earth and Planetary Interiors*, *312*, 106655. doi: 10.1016/j.pepi.2021.106655

Genda, H., Brasser, R., & Mojzsis, S. J. (2017, December). The terrestrial late veneer from core disruption of a lunar-sized impactor. *Earth and Planetary Science Letters*, *480*, 25-32. doi: 10.1016/j.epsl.2017.09.041

Gladman, B. J., Davis, D. R., Neese, C., Jedicke, R., Williams, G., Kavelaars, J. J., ... Tricarico, P. (2009, July). On the asteroid belt's orbital and size distribution. *Icarus*, *202*(1), 104-118. doi: 10.1016/j.icarus.2009.02.012

Goderis, S., Sato, H., Ferrière, L., Schmitz, B., Burney, D., Kaskes, P., ... Whalen, M. T. (2021, February). Globally distributed iridium layer preserved within the Chicxulub impact structure. *Science Advances*, *7*(9), eabe3647. doi: 10.1126/sciadv.abe3647

Grewal, D. S., Nie, N. X., Zhang, B., Izidoro, A., & Asimow, P. D. (2024, March). Accretion of the earliest inner Solar System planetesimals beyond the water snowline. *Nature Astronomy*, *8*, 290-297. doi: 10.1038/s41550-023-02172-w

Hamano, K., Abe, Y., & Genda, H. (2013, May). Emergence of two types of terrestrial planet on solidification of magma ocean. *Nature*, *497*(7451), 607-610. doi: 10.1038/nature12163

Hinze, J. O. (1955). Fundamentals of the hydrodynamic mechanism of splitting in dispersion processes. *AIChE journal*, *1*(3), 289–295.

Ita, J., & Cohen, R. E. (1998). Diffusion in mgo at high pressure: Implications for lower mantle rheology. *Geophysical research letters*, *25*(7), 1095–1098.

Itcovitz, J. P., Rae, A. S. P., Davison, T. M., Collins, G. S., & Shorttle, O. (2024, April). The Distribution of Impactor Core Material During Large Impacts on Earth-like Planets. *The Planetary Science Journal*, *5*(4), 90. doi: 10.3847/PSJ/ad2ea4

Jackson, A. P., Perera, V., & Gabriel, T. S. J. (2023, April). Impact Generation of Holes in the Early Lunar Crust: Scaling Relations. *Journal of Geophysical Research (Planets)*, *128*(4), e2022JE007498. doi: 10.1029/2022JE007498

Jacobson, S. A., Morbidelli, A., Raymond, S. N., O'Brien, D. P., Walsh, K. J., & Rubie, D. C. (2014, April). Highly siderophile elements in Earth's mantle as a clock for the Moon-forming impact. *Nature*, *508*(7494), 84-87. doi: 10.1038/nature13172

Jarvis, G. T., & Peltier, W. (1982). Mantle convection as a boundary layer phenomenon. *Geophysical Journal International*, *68*(2), 389–427.

Johansen, A., Mac Low, M.-M., Lacerda, P., & Bizzarro, M. (2015, April). Growth of asteroids, planetary embryos, and Kuiper belt objects by chondrule accretion. *Science Advances*, *1*, 1500109. doi: 10.1126/sciadv.1500109

Johnson, B. C., & Melosh, H. J. (2012, January). Formation of spherules in impact produced vapor plumes. *Icarus*, *217*(1), 416-430. doi: 10.1016/j.icarus.2011.11.020

Joiret, S., Raymond, S. N., Avice, G., & Clement, M. S. (2024, May). Crash Chronicles: Relative contribution from comets and carbonaceous asteroids to Earth's volatile budget in the context of an Early Instability. *Icarus*, *414*, 116032. doi: 10.1016/j.icarus.2024.116032

Karato, S.-i., & Rama Murthy, V. (1997, March). Core formation and chemical equilibrium in the Earth—I. Physical considerations. *Physics of the Earth and Planetary Interiors*, *100*(1), 61-79. doi: 10.1016/S0031-9201(96)03232-3

Karki, B. B., & Stixrude, L. P. (2010). Viscosity of mgsio3 liquid at earth's mantle conditions: Implications for an early magma ocean. *Science*, *328*(5979), 740–742.

Kendall, J. D., & Melosh, H. J. (2016, August). Differentiated planetesimal impacts into a terrestrial magma ocean: Fate of the iron core. *Earth and Planetary Science Letters*, *448*, 24-33. doi: 10.1016/j.epsl.2016.05.012

Kimura, K., Lewis, R. S., & Anders, E. (1974, May). Distribution of gold and rhenium between nickel-iron and silicate melts: implications for the abundance of siderophile elements on the Earth and Moon. *Geochimica et Cosmochimica Acta*, *38*(5), 683-701. doi: 10.1016/0016-7037(74)90144-6

Kleine, T., Palme, H., Mezger, K., & Halliday, A. N. (2005, December). Hf-W Chronometry of Lunar Metals and the Age and Early Differentiation of the Moon. *Science*, *310*(5754), 1671-1674. doi: 10.1126/science.1118842

Kleine, T., Touboul, M., Bourdon, B., Nimmo, F., Mezger, K., Palme, H., ... Halliday, A. N. (2009, September). Hf-W chronology of the accretion and early evolution of asteroids and terrestrial planets. *Geochimica et Cosmochimica Acta*, *73*(17), 5150-5188. doi: 10.1016/j.gca.2008.11.047

Korenaga, J. (2018, November). Crustal evolution and mantle dynamics through Earth history. *Philosophical Transactions of the Royal Society of London Series A*, *376*(2132), 20170408. doi: 10.1098/rsta.2017.0408

Korenaga, J., & Marchi, S. (2023). Vestiges of impact-driven three-phase mixing in the chemistry and structure of earth's mantle. *Proceedings of the National Academy of Sciences*, *120*(43), e2309181120. Retrieved from `https://www.pnas.org/doi/abs/10.1073/pnas.2309181120` doi: 10.1073/pnas.2309181120

Kraus, R. G., Root, S., Lemke, R. W., Stewart, S. T., Jacobsen, S. B., & Mattsson, T. R. (2015, April). Impact vaporization of planetesimal cores in the late stages of planet formation. *Nature Geoscience*, *8*(4), 269-272. doi: 10.1038/ngeo2369

Kruijer, T. S., Kleine, T., Fischer-Gödde, M., & Sprung, P. (2015, April). Lunar tungsten isotopic evidence for the late veneer. *Nature*, *520*(7548), 534-537. doi: 10.1038/nature14360

Labrosse, S., Morison, A., & Tackley, P. J. (2024). Solid-state mantle convection coupled with a crystallising basal magma ocean. *Comptes Rendus. Géoscience*, *356*(S1), 5–21. doi: 10.5802/crgeos.275

Landeau, M., Deguen, R., Phillips, D., Neufeld, J. A., Lherm, V., & Dalziel, S. B. (2021, June). Metal-silicate mixing by large Earth-forming impacts. *Earth and Planetary Science Letters*, *564*, 116888. doi: 10.1016/j.epsl.2021.116888

Lavorel, G., & Le Bars, M. (2009, October). Sedimentation of particles in a vigorously convecting fluid. *Physical Review E*, *80*(4), 046324. doi: 10.1103/PhysRevE.80.046324

Lebrun, T., Massol, H., Chassefière, E., Davaille, A., Marcq, E., Sarda, P., ... Brandeis, G. (2013). Thermal evolution of an early magma ocean in interaction with the atmosphere. *Journal of Geophysical Research: Planets*, *118*(6), 1155–1176.

Lejeune, A.-M., & Richet, P. (1995). Rheology of crystal-bearing silicate melts: An experimental study at high viscosities. *Journal of Geophysical Research: Solid Earth*, *100*(B3), 4215–4229.

Lherm, V., & Deguen, R. (2018, December). Small-Scale Metal/Silicate Equilibration During Core Formation: The Influence of Stretching Enhanced Diffusion on Mixing. *Journal of Geophysical Research (Solid Earth)*, *123*(12), 10,496-10,516. doi: 10.1029/2018JB016537

Li, Z., Caracas, R., & Soubiran, F. (2020, October). Partial core vaporization during Giant Impacts inferred from the entropy and the critical point of iron. *Earth and Planetary Science Letters*, *547*, 116463. doi: 10.1016/j.epsl.2020.116463

Lissauer, J. J., Squyres, S. W., & Hartmann, W. K. (1988, November). Bombardment history of the Saturn system. *Journal of Geophysical Research*, *93*, 13776-13804. doi: 10.1029/JB093iB11p13776

Lock, S. J., Stewart, S. T., Petaev, M. I., Leinhardt, Z., Mace, M. T., Jacobsen, S. B., & Cuk, M. (2018, April). The Origin of the Moon Within a Terrestrial Synestia. *Journal of Geophysical Research (Planets)*, *123*(4), 910-951. doi: 10.1002/2017JE005333

Maller, A., Landeau, M., Allibert, L., & Charnoz, S. (2024). Condition for metal fragmentation during earth-forming collisions. *Physics of the Earth and Planetary Interiors*, *352*, 107199. Retrieved from `https://www.sciencedirect.com/science/article/pii/S0031920124000578` doi: https://doi.org/10.1016/j.pepi.2024.107199

Mann, U., Frost, D. J., Rubie, D. C., Becker, H., & Audétat, A. (2012, May). Partitioning of Ru, Rh, Pd, Re, Ir and Pt between liquid metal and silicate at high pressures and high temperatures - Implications for the origin of highly siderophile element concentrations in the Earth's mantle. *Geochimica et Cosmochimica Acta*, *84*, 593-613. doi: 10.1016/j.gca.2012.01.026

Marchi, S., Bottke, W. F., Elkins-Tanton, L. T., Bierhaus, M., Wuennemann, K., Morbidelli, A., & Kring, D. A. (2014, July). Widespread mixing and burial of Earth's Hadean crust by asteroid impacts. *Nature*, *511*(7511), 578-582. doi: 10.1038/nature13539

Marchi, S., Canup, R. M., & Walker, R. J. (2018, December). Heterogeneous delivery of silicate and metal to the Earth by large planetesimals. *Nature Geoscience*, *11*(1), 77-81. doi: 10.1038/s41561-017-0022-3

Martins, R., Kuthning, S., Coles, B. J., Kreissig, K., & Rehkämper, M. (2023, January). Nucleosynthetic isotope anomalies of zinc in meteorites constrain the origin of Earth's volatiles. *Science*, *379*(6630), 369-372. doi: 10.1126/science.abn1021

Martins, R., Morton, E. M., Kuthning, S., Goes, S., Williams, H. M., & Rehkämper, M. (2024, October). Primitive asteroids as a major source of terrestrial volatiles. *Science Advances*, *10*(41), eado4121. doi: 10.1126/sciadv.ado4121

Marty, B. (2012, January). The origins and concentrations of water, carbon, nitrogen and noble gases on Earth. *Earth and Planetary Science Letters*, *313*, 56-66. doi: 10.1016/j.epsl.2011.10.040

Masiero, J. R., Mainzer, A. K., Grav, T., Bauer, J. M., Cutri, R. M., Dailey, J., ... Wilkins, A. (2011, November). Main Belt Asteroids with WISE/NEOWISE. I. Preliminary Albedos and Diameters. *The Astrophysical Journal*, *741*(2), 68. doi: 10.1088/0004-637X/741/2/68

Maurice, M., Tosi, N., Samuel, H., Plesa, A.-C., Hüttig, C., & Breuer, D. (2017, March). Onset of solid-state mantle convection and mixing during magma ocean solidification. *Journal of Geophysical Research (Planets)*, *122*(3), 577-598. doi: 10.1002/2016JE005250

Melosh, H., & Collins, G. (2005). Meteor crater formed by low-velocity impact. *Nature*, *434*(7030), 157–157.

Melosh, H. J. (1989). *Impact cratering : a geologic process.*

Miller, G. H., Stolper, E. M., & Ahrens, T. J. (1991, JUL 10). The equation of state of a molten komatiite.1. shock-wave compression to 36 gpa [Article]. *J. Geophys. Res.*, *96*(B7), 11831-11848. doi: {10.1029/91JB01204}

Mojzsis, S. J., Brasser, R., Kelly, N. M., Abramov, O., & Werner, S. C. (2019, August). Onset of Giant Planet Migration before 4480 Million Years Ago. *The*

Astrophysical Journal, *881*(1), 44. doi: 10.3847/1538-4357/ab2c03

Monteux, J., Qaddah, B., & Andrault, D. (2023, May). Conditions for Segregation of a Crystal-Rich Layer Within a Convective Magma Ocean. *Journal of Geophysical Research (Planets)*, *128*(5). doi: 10.1029/2023JE007805

Morard, G., Siebert, J., Andrault, D., Guignot, N., Garbarino, G., Guyot, F., & Antonangeli, D. (2013). The earth's core composition from high pressure density measurements of liquid iron alloys. *Earth Planet. Sci. Lett.*, *373*, 169-178.

Morbidelli, A., Bottke, W. F., Nesvorný, D., & Levison, H. F. (2009, December). Asteroids were born big. *Icarus*, *204*(2), 558-573. doi: 10.1016/j.icarus.2009.07.011

Morbidelli, A., Nesvorny, D., Laurenz, V., Marchi, S., Rubie, D. C., Elkins-Tanton, L., . . . Jacobson, S. (2018, May). The timeline of the lunar bombardment: Revisited. *Icarus*, *305*, 262-276. doi: 10.1016/j.icarus.2017.12.046

Morison, A., Labrosse, S., Deguen, R., & Alboussière, T. (2019, June). Timescale of overturn in a magma ocean cumulate. *Earth and Planetary Science Letters*, *516*, 25-36. doi: 10.1016/j.epsl.2019.03.037

Nakajima, M., Golabek, G. J., Wünnemann, K., Rubie, D. C., Burger, C., Melosh, H. J., . . . Hull, S. D. (2021, August). Scaling laws for the geometry of an impact-induced magma ocean. *Earth and Planetary Science Letters*, *568*, 116983. doi: 10.1016/j.epsl.2021.116983

Nakajima, M., & Stevenson, D. J. (2015, October). Melting and mixing states of the Earth's mantle after the Moon-forming impact. *Earth and Planetary Science Letters*, *427*, 286-295. doi: 10.1016/j.epsl.2015.06.023

Nimmo, F., Kleine, T., & Morbidelli, A. (2024, December). Tidally driven remelting around 4.35 billion years ago indicates the Moon is old. *Nature*, *636*(8043), 598-602. doi: 10.1038/s41586-024-08231-0

Olson, P., & Weeraratne, D. (2008). Experiments on metal–silicate plumes and core formation. *Philosophical Transactions of the Royal Society A: Mathematical, Physical and Engineering Sciences*, *366*(1883), 4253–4271.

Pahlevan, K., & Morbidelli, A. (2015, November). Collisionless encounters and the origin of the lunar inclination. *Nature*, *527*(7579), 492-494. doi: 10.1038/nature16137

Passey, Q. R., & Melosh, H. J. (1980, May). Effects of atmospheric breakup on crater field formation. *Icarus*, *42*(2), 211-233. doi: 10.1016/0019-1035(80)90072-X

Pierazzo, E., & Melosh, H. J. (2000, January). Hydrocode modeling of oblique impacts: The fate of the projectile. *Meteoritics & Planetary Science*, *35*(1), 117-130. doi: 10.1111/j.1945-5100.2000.tb01979.x

Pierazzo, E., Vickery, A., & Melosh, H. (1997). A reevaluation of impact melt production. *Icarus*, *127*(2), 408–423.

Potter, R. W. K., & Collins, G. S. (2013, May). Numerical modeling of asteroid survivability and possible scenarios for the Morokweng crater-forming impact. *Meteoritics & Planetary Science*, *48*(5), 744-757. doi: 10.1111/maps.12098

Raymond, S. N., Schlichting, H. E., Hersant, F., & Selsis, F. (2013, September). Dynamical and collisional constraints on a stochastic late veneer on the terrestrial planets. *Icarus*, *226*(1), 671-681. doi: 10.1016/j.icarus.2013.06.019

Righter, K., Humayun, M., & Danielson, L. (2008, May). Partitioning of palladium at high pressures and temperatures during core formation. *Nature Geoscience*, *1*(5), 321-323. doi: 10.1038/ngeo180

Rimmer, P. B., Shorttle, O., & Rugheimer, S. (2019). Oxidised micrometeorites as evidence for low atmospheric pressure on the early earth. *Geochemical Perspectives Letters*, *9*, 38-42. Retrieved from `https://www.geochemicalperspectivesletters.org/article1903`

Rivière, A., Ruth, D. J., Mostert, W., Deike, L., & Perrard, S. (2022, August). Capillary driven fragmentation of large gas bubbles in turbulence. *Physical Review*

Fluids, *7*(8), 083602. doi: 10.1103/PhysRevFluids.7.083602
Roberts, J. H., & Zhong, S. (2006, June). Degree-1 convection in the Martian mantle and the origin of the hemispheric dichotomy. *Journal of Geophysical Research (Planets)*, *111*(E6), E06013. doi: 10.1029/2005JE002668
Rosas, J. C., & Korenaga, J. (2018, July). Rapid crustal growth and efficient crustal recycling in the early Earth: Implications for Hadean and Archean geodynamics. *Earth and Planetary Science Letters*, *494*, 42-49. doi: 10.1016/j.epsl.2018.04.051
Rubie, D. C., Laurenz, V., Jacobson, S. A., Morbidelli, A., Palme, H., Vogel, A. K., & Frost, D. J. (2016, September). Highly siderophile elements were stripped from Earth's mantle by iron sulfide segregation. *Science*, *353*(6304), 1141-1144. doi: 10.1126/science.aaf6919
Rubie, D. C., Melosh, H. J., Reid, J. E., Liebske, C., & Righter, K. (2003, January). Mechanisms of metal-silicate equilibration in the terrestrial magma ocean. *Earth and Planetary Science Letters*, *205*(3-4), 239-255. doi: 10.1016/S0012-821X(02)01044-0
Ryder, G. (2002, April). Mass flux in the ancient Earth-Moon system and benign implications for the origin of life on Earth. *Journal of Geophysical Research (Planets)*, *107*(E4), 5022. doi: 10.1029/2001JE001583
Salvador, A., Massol, H., Davaille, A., Marcq, E., Sarda, P., & Chassefière, E. (2017, July). The relative influence of H_2O and CO_2 on the primitive surface conditions and evolution of rocky planets. *Journal of Geophysical Research (Planets)*, *122*(7), 1458-1486. doi: 10.1002/2017JE005286
Salvador, A., & Samuel, H. (2023, January). Convective outgassing efficiency in planetary magma oceans: Insights from computational fluid dynamics. *Icarus*, *390*, 115265. doi: 10.1016/j.icarus.2022.115265
Samuel, H. (2012, January). A re-evaluation of metal diapir breakup and equilibration in terrestrial magma oceans. *Earth and Planetary Science Letters*, *313*, 105-114. doi: 10.1016/j.epsl.2011.11.001
Saurety, A., Caracas, R., & Raymond, S. N. (2025, March). Impact-induced Vaporization during Accretion of Planetary Bodies. *The Astrophysical Journal Letters*, *981*(1), L13. doi: 10.3847/2041-8213/adb30e
Schlichting, H. E., Warren, P. H., & Yin, Q.-Z. (2012, June). The Last Stages of Terrestrial Planet Formation: Dynamical Friction and the Late Veneer. *The Astrophysical Journal*, *752*(1), 8. doi: 10.1088/0004-637X/752/1/8
Schubert, G., Zhang, K., Kivelson, M. G., & Anderson, J. D. (1996, December). The magnetic field and internal structure of Ganymede. *Nature*, *384*(6609), 544-545. doi: 10.1038/384544a0
Scott, E. R. D., & Krot, A. N. (2003, December). Chondrites and their Components. *Treatise on Geochemistry*, *1*, 711. doi: 10.1016/B0-08-043751-6/01145-2
Shraiman, B. I., & Siggia, E. D. (1990). Heat transport in high-rayleigh-number convection. *Physical Review A*, *42*(6), 3650.
Simon, J. B., Armitage, P. J., Li, R., & Youdin, A. N. (2016, May). The Mass and Size Distribution of Planetesimals Formed by the Streaming Instability. I. The Role of Self-gravity. *The Astrophysical Journal*, *822*(1), 55. doi: 10.3847/0004-637X/822/1/55
Solomatov, V. (2015). Magma oceans and primordial mantle differentiation. *Treatise on geophysics, Earth Formation and Evolution*, *9*, 91–119.
Solomatov, V. S. (2000). Fluid dynamics of a terrestrial magma ocean. *Origin of the Earth and Moon*, *1*, 323–338.
Solomatov, V. S., Olson, P., & Stevenson, D. J. (1993). Entrainment from a bed of particles by thermal convection. *Earth and planetary science letters*, *120*(3-4), 387–393.
Solomatov, V. S., & Stevenson, D. J. (1993). Suspension in convective layers and style of differentiation of a terrestrial magma ocean. *Journal of Geophysical*

Research: Planets, *98*(E3), 5375–5390.
Stebbins, J., Carmichael, I., & Moret, L. (1984). Heat capacities and entropies of silicate liquids and glasses. *Contributions to mineralogy and petrology*, *86*, 131–148.
Steenstra, E. S., Berndt, J., Klemme, S., Snape, J. F., Bullock, E. S., & van Westrenen, W. (2020, November). The Fate of Sulfur and Chalcophile Elements During Crystallization of the Lunar Magma Ocean. *Journal of Geophysical Research (Planets)*, *125*(11), e06328. doi: 10.1029/2019JE006328
Sturtz, C., Kaminski, É., Limare, A., & Tait, S. (2021). The fate of particles in a volumetrically heated convective fluid at high prandtl number. *Journal of Fluid Mechanics*, *929*, A28.
Suer, T.-A., Siebert, J., Remusat, L., Day, J. M. D., Borensztajn, S., Doisneau, B., & Fiquet, G. (2021, January). Reconciling metal-silicate partitioning and late accretion in the Earth. *Nature Communications*, *12*, 2913. doi: 10.1038/s41467-021-23137-5
Svetsov, V., Nemtchinov, I., & Teterev, A. (1995). Disintegration of large meteoroids in earth's atmosphere: Theoretical models. *Icarus*, *116*(1), 131–153.
Thomas, P. C., Parker, J. W., McFadden, L. A., Russell, C. T., Stern, S. A., Sykes, M. V., & Young, E. F. (2005, September). Differentiation of the asteroid Ceres as revealed by its shape. *Nature*, *437*(7056), 224-226. doi: 10.1038/nature03938
Tonks, W. B., & Melosh, H. J. (1993, March). Magma ocean formation due to giant impacts. *Journal of Geophysical Research*, *98*(E3), 5319-5333. doi: 10.1029/92JE02726
Touboul, M., Kleine, T., Bourdon, B., Palme, H., & Wieler, R. (2007, December). Late formation and prolonged differentiation of the Moon inferred from W isotopes in lunar metals. *Nature*, *450*(7173), 1206-1209. doi: 10.1038/nature06428
Touboul, M., Puchtel, I. S., & Walker, R. J. (2015, April). Tungsten isotopic evidence for disproportional late accretion to the Earth and Moon. *Nature*, *520*(7548), 530-533. doi: 10.1038/nature14355
Turcotte, D. L., & Schubert, G. (2002). *Geodynamics*. Cambridge university press.
Ulvrová, M., Coltice, N., Ricard, Y., Labrosse, S., Dubuffet, F., VelíMský, J., & Å RáMek, O. (2011, October). Compositional and thermal equilibration of particles, drops, and diapirs in geophysical flows. *Geochemistry, Geophysics, Geosystems*, *12*(10), Q10014. doi: 10.1029/2011GC003757
Valley, J. W., Cavosie, A. J., Ushikubo, T., Reinhard, D. A., Lawrence, D. F., Larson, D. J., … Spicuzza, M. J. (2014, March). Hadean age for a post-magma-ocean zircon confirmed by atom-probe tomography. *Nature Geoscience*, *7*(3), 219-223. doi: 10.1038/ngeo2075
Wacheul, J.-B., & Le Bars, M. (2018, March). Experiments on fragmentation and thermo-chemical exchanges during planetary core formation. *Physics of the Earth and Planetary Interiors*, *276*, 134-144. doi: 10.1016/j.pepi.2017.05.018
Walker, R. J. (2009, June). Highly siderophile elements in the Earth, Moon and Mars: Update and implications for planetary accretion and differentiation. *Chemie der Erde / Geochemistry*, *69*(2), 101-125. doi: 10.1016/j.chemer.2008.10.001
Weidenschilling, S. J. (2011, August). Initial sizes of planetesimals and accretion of the asteroids. *Icarus*, *214*(2), 671-684. doi: 10.1016/j.icarus.2011.05.024
Wieczorek, M. A., Neumann, G. A., Nimmo, F., Kiefer, W. S., Taylor, G. J., Melosh, H. J., … Zuber, M. T. (2013, February). The Crust of the Moon as Seen by GRAIL. *Science*, *339*(6120), 671-675. doi: 10.1126/science.1231530
Woo, J. M. Y., Nesvorný, D., Scora, J., & Morbidelli, A. (2024, July). Terrestrial planet formation from a ring: Long-term simulations accounting for the giant planet instability. *Icarus*, *417*, 116109. doi: 10.1016/j.icarus.2024.116109

Wood, J. A., Dickey, J. S., Jr., Marvin, U. B., & Powell, B. N. (1970, January). Lunar anorthosites and a geophysical model of the moon. *Geochimica et Cosmochimica Acta Supplement*, *1*, 965.

Wünnemann, K., Collins, G., & Osinski, G. (2008). Numerical modelling of impact melt production in porous rocks. *Earth and Planetary Science Letters*, *269*(3), 530-539. Retrieved from `https://www.sciencedirect.com/science/article/pii/S0012821X08001660` doi: https://doi.org/10.1016/j.epsl.2008.03.007